Chapter 14

Turbulence in Stratified Fluids

ABSTRACT
The previous chapter treated organized wave flows in stratified fluids, whereas the attention now turns to more complicated motions, such as vertical mixing, flow instability, forced turbulence, and convection. Because the study of such phenomena does not lend itself to analytical solutions, the emphasis is on budgets and scale analysis. The numerical section presents a few methods by which mixing and turbulence can be represented in numerical models.

14.1 MIXING OF STRATIFIED FLUIDS

Mixing by turbulence generates vertical motions and overturning. In a homogeneous fluid, the required energy is only that necessary to overcome mechanical friction (see Sections 5.1 and 8.1), but in a stratified fluid, work must also be performed to raise heavy fluid parcels and lower light parcels. Let us consider, for example, the system pictured in Fig. 14.1. Initially, it consists of two layers of equal thicknesses with fluids of different densities and horizontal velocities. After some time, mixing is assumed to have taken place, and the system consists of a single layer of average density flowing with the average velocity.[1] Because the heavier fluid (density ρ_2) lies initially below the lighter fluid (density ρ_1), the initial center of gravity is below mid-depth level, whereas in the final state, it is exactly at mid-depth. Thus, the center of gravity has been raised in the mixing process, and potential energy must have been provided to the system. Put another way, work has been performed against the buoyancy forces. With identical initial depths $H_1 = H_2 = H/2$, the average density is $\rho = (\rho_1 + \rho_2)/2$, and the potential energy gain is

$$PE\,\text{gain} = \int_0^H \rho_{\text{final}}\, gz\, \mathrm{d}z - \int_0^H \rho_{\text{initial}}\, gz\, \mathrm{d}z$$

[1] Credit for this illustrative example goes to Prof. William K. Dewar.

Introduction to Geophysical Fluid Dynamics, Volume 101, ISSN 0074-6142, DOI: 10.1016/B978-0-12-088759-0.00014-8
Copyright © 2011, Elsevier Inc. All rights reserved.

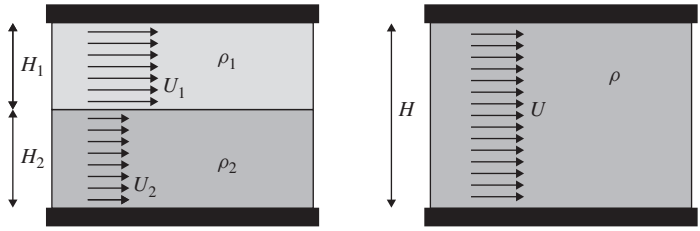

FIGURE 14.1 Mixing of a two-layer stratified fluid with velocity shear. Rising of dense fluid and lowering of light fluid both require work against buoyancy forces and thus lead to an increase in potential energy. Concomitantly, the kinetic energy of the system decreases during mixing. Only when the kinetic-energy drop exceeds the potential-energy rise can mixing proceed spontaneously.

$$= \frac{1}{2}\rho g H^2 - \left[\frac{1}{2}\rho_2 g\frac{H^2}{4} + \frac{1}{2}\rho_1 g\frac{3H^2}{4}\right]$$

$$= \frac{1}{8}(\rho_2 - \rho_1) g H^2. \tag{14.1}$$

The question arises as to the source of this energy increase. Because human intervention is ruled out in geophysical flows, a natural energy supply must exist or mixing would not take place. In this case, kinetic energy is released in the mixing process, as long as the initial velocity distribution is nonuniform. Conservation of momentum in the absence of external forces and in the context of the Boussinesq approximation ($\rho_1 \simeq \rho_2 \simeq \rho_0$) implies that the final, uniform velocity is the average of the initial velocities: $U = (U_1 + U_2)/2$. This indeed leads to a kinetic-energy loss

$$KE \text{ loss} = \int_0^H \frac{1}{2}\rho_0 u_{\text{initial}}^2 \mathrm{d}z - \int_0^H \frac{1}{2}\rho_0 u_{\text{final}}^2 \mathrm{d}z$$

$$= \frac{1}{2}\rho_0 U_2^2 \frac{H}{2} + \frac{1}{2}\rho_0 U_1^2 \frac{H}{2} - \frac{1}{2}\rho_0 U^2 H$$

$$= \frac{1}{8}\rho_0 (U_1 - U_2)^2 H. \tag{14.2}$$

Complete vertical mixing is naturally possible only if the kinetic-energy loss exceeds the potential-energy gain; that is,

$$\frac{(\rho_2 - \rho_1) g H}{\rho_0 (U_1 - U_2)^2} < 1. \tag{14.3}$$

Physically, the initial density difference should be sufficiently weak in order not to present an insurmountable gravitational barrier, or alternatively the initial

velocity shear should be sufficiently large to supply the necessary amount of energy. When criterion (14.3) is not satisfied, mixing occurs only in the vicinity of the initial interface and cannot extend over the entire system. The determination of the characteristics of such localized mixing calls for a more detailed analysis.

For this purpose, let us now consider a two-fluid system of infinite extent (Fig. 14.2), with upper and lower densities and velocities denoted, respectively, by ρ_1, ρ_2 and U_1, U_2, and let us explore interfacial waves of infinitesimal

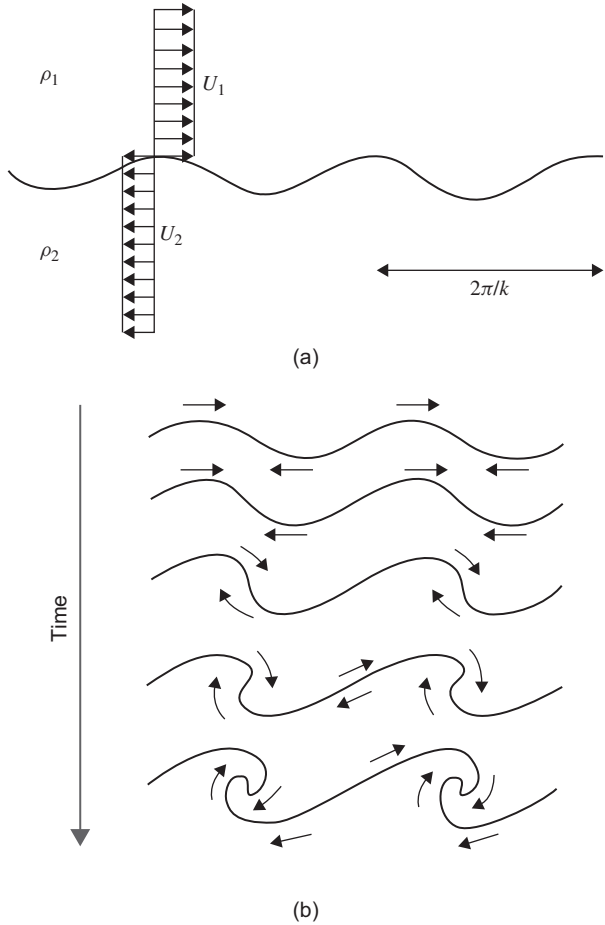

FIGURE 14.2 Kelvin–Helmholtz instability: (a) initial perturbation of wavenumber k, (b) temporal evolution of an unstable perturbation. The system is always unstable to short waves, which steepen, overturn, and ultimately cause mixing. As waves overturn, their vertical and lateral dimensions are comparable.

amplitudes. Mathematical derivations, not reproduced here, show that a sinusoidal perturbation of wavenumber k (corresponding to wavelength $2\pi/k$) is unstable if (Kundu, 1990, Section 11.6)

$$(\rho_2^2 - \rho_1^2)g < \rho_1\rho_2 k(U_1 - U_2)^2, \tag{14.4}$$

or for a Boussinesq fluid ($\rho_1 \simeq \rho_2 \simeq \rho_0$),

$$2(\rho_2 - \rho_1)g < \rho_0 k(U_1 - U_2)^2. \tag{14.5}$$

In a stability analysis, waves of all wavelengths must be considered, and we conclude that there will always be sufficiently short waves to cause instabilities. Therefore, a two-layer shear flow is always unstable. This is known as the *Kelvin–Helmholtz instability*. Among other instances, this instability plays a role in the generation of water waves by surface winds.

The details of the analysis leading to Eq. (14.5) reveal that the interfacial waves induce flow perturbations that extend on both sides of the interface across a height on the order of their wavelength. Thus, as unstable waves grow, they form rolls of height comparable to their width (Figs. 14.2, 14.3, and 14.4).

The rolling and breaking of waves induces turbulent mixing, and it is expected that the vertical extent of the mixing zone, which we denote by ΔH, scales like the wavelength of the longest unstable wave, that for which criterion (14.5) turns into an equality:

$$\Delta H \sim \frac{1}{k_{\min}} = \frac{\rho_0(U_1 - U_2)^2}{2(\rho_2 - \rho_1)g}. \tag{14.6}$$

If the fluid system is of finite depth H, the preceding theory is no longer applicable, but we can anticipate, by virtue of dimensional analysis, that the results still hold, within some numerical factors. For a fluid depth H greater than ΔH, mixing must remain localized to a band of thickness ΔH, whereas for a fluid depth H less than ΔH, that is,

$$H \lesssim \frac{\rho_0(U_1 - U_2)^2}{(\rho_2 - \rho_1)g}, \tag{14.7}$$

mixing will engulf the entire system. Note the similarity between this last inequality, derived from a wave theory, and inequality (14.3) obtained from energy considerations.

Figures 14.5 and 14.6 show atmospheric instances of Kelvin–Helmholtz instabilities made visible by localized cloud formation. Kelvin–Helmholtz instabilities have also been observed to take place in the ocean (Woods, 1968).

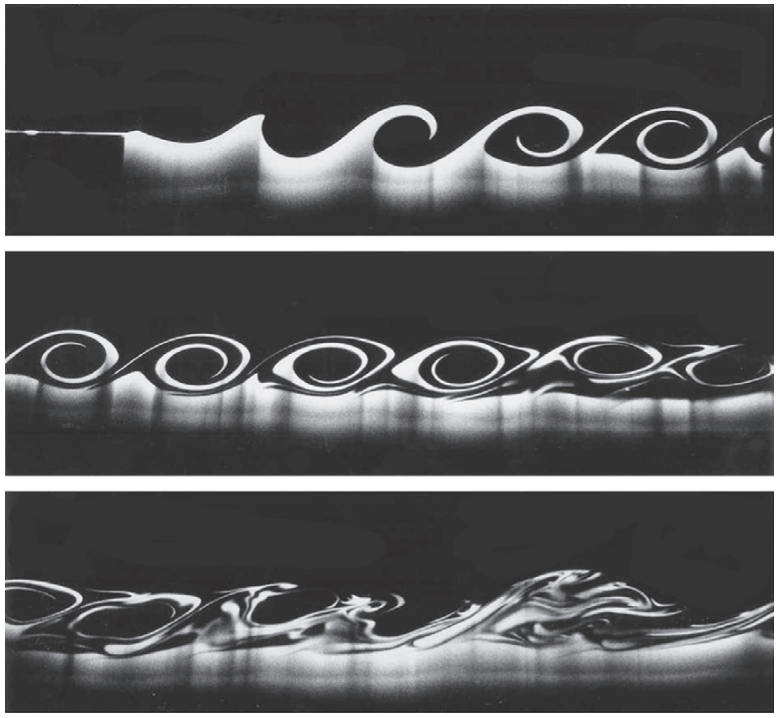

FIGURE 14.3 Development of a Kelvin–Helmholtz instability in the laboratory. Here, two layers flowing from left to right join downstream of a thin plate (visible on the left of the top photograph). The upper and faster moving layer is slightly less dense than the lower layer. Downstream distance (from left to right on each photograph and from top to bottom panel) plays the role of time. At first, waves form and overturn in a two-dimensional fashion (in the vertical plane of the photo), but eventually, three-dimensional motions appear that lead to turbulence and complete the mixing. (*Courtesy of Greg A. Lawrence. For more details on the laboratory experiment, see Lawrence, Browand & Redekopp, 1991*)

14.2 INSTABILITY OF A STRATIFIED SHEAR FLOW: THE RICHARDSON NUMBER

In the preceding section, we restricted our considerations to a discontinuity of the density and horizontal velocity, only to find that such a discontinuous stratification is always unstable. Instability causes mixing, and mixing will proceed until the velocity profile has been made stable. The question then is as follows: For a gradual density stratification, what is the critical velocity shear below which the system is stable and above which mixing occurs? To answer this question, we are led to study the stability of a stratified shear flow.

Let us consider a two-dimensional (x, z) inviscid and nondiffusive fluid with horizontal and vertical velocities (u, w), dynamic pressure p, and density

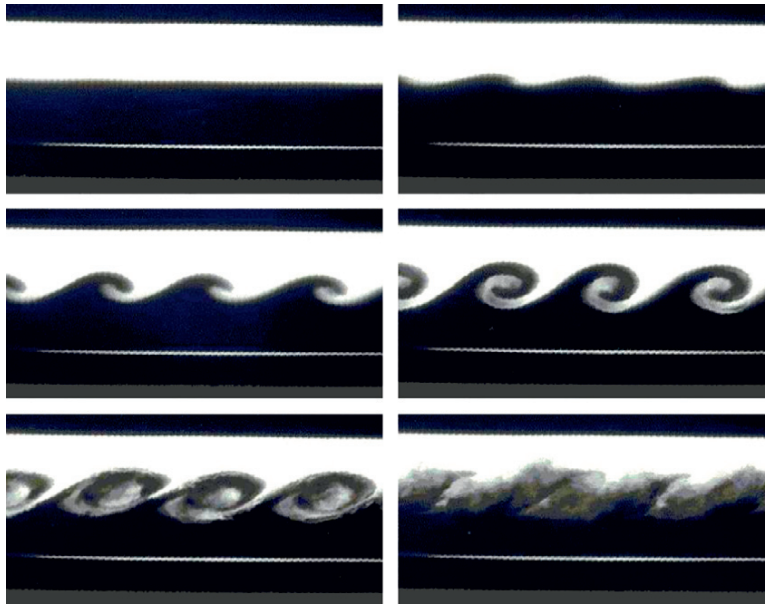

FIGURE 14.4 Kelvin–Helmholtz instability generated in a laboratory with fluids of two different densities and colors. (*Adapted from GFD-online, Satoshi Sakai, Isawo Iizawa, Eiji Aramaki*)

FIGURE 14.5 Kelvin–Helmholtz instability in the Algerian sky. (*Photo by one of the authors*).

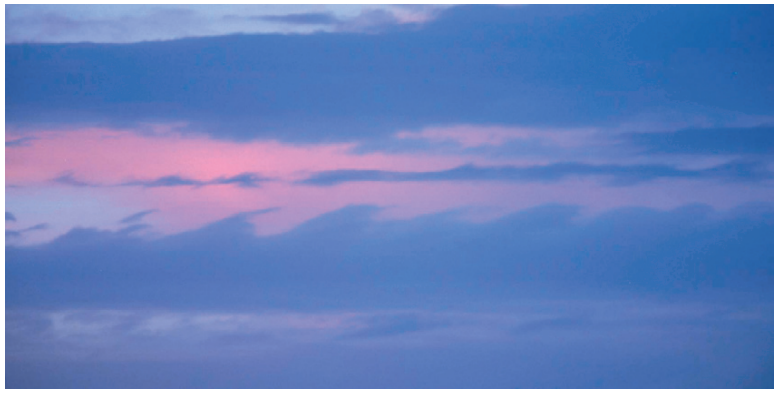

FIGURE 14.6 Kelvin–Helmholtz instability over the Sahara desert. (*Photo by one of the authors*)

anomaly ρ. In anticipation of the important role played by vertical motions, we reinstate the acceleration term in the vertical momentum equation (Section 4.3) and write

$$\frac{\partial u}{\partial t}+u\frac{\partial u}{\partial x}+w\frac{\partial u}{\partial z}=-\frac{1}{\rho_0}\frac{\partial p}{\partial x} \tag{14.8a}$$

$$\frac{\partial w}{\partial t}+u\frac{\partial w}{\partial x}+w\frac{\partial w}{\partial z}=-\frac{1}{\rho_0}\frac{\partial p}{\partial z}-\frac{\rho g}{\rho_0} \tag{14.8b}$$

$$\frac{\partial u}{\partial x}+\frac{\partial w}{\partial z}=0 \tag{14.8c}$$

$$\frac{\partial \rho}{\partial t}+u\frac{\partial \rho}{\partial x}+w\frac{\partial \rho}{\partial z}=0. \tag{14.8d}$$

Our basic state consists of a steady, sheared horizontal flow $[u=\bar{u}(z),\ w=0]$ in a vertical density stratification $[\rho=\bar{\rho}(z)]$. The accompanying pressure field $\bar{p}(z)$ obeys $\mathrm{d}\bar{p}/\mathrm{d}z=-g\bar{\rho}(z)$. The addition of an infinitesimally small perturbation $(u=\bar{u}+u',\ w=w',\ p=\bar{p}+p',\ \rho=\bar{\rho}+\rho')$ and a subsequent linearization of the equations yield

$$\frac{\partial u'}{\partial t}+\bar{u}\frac{\partial u'}{\partial x}+w'\frac{\mathrm{d}\bar{u}}{\mathrm{d}z}=-\frac{1}{\rho_0}\frac{\partial p'}{\partial x} \tag{14.9a}$$

$$\frac{\partial w'}{\partial t}+\bar{u}\frac{\partial w'}{\partial x}=-\frac{1}{\rho_0}\frac{\partial p'}{\partial z}-\frac{\rho' g}{\rho_0} \tag{14.9b}$$

$$\frac{\partial u'}{\partial x}+\frac{\partial w'}{\partial z}=0 \tag{14.9c}$$

$$\frac{\partial \rho'}{\partial t}+\bar{u}\frac{\partial \rho'}{\partial x}+w'\frac{\mathrm{d}\bar{\rho}}{\mathrm{d}z}=0. \tag{14.9d}$$

Introducing the perturbation streamfunction ψ via $u' = +\partial\psi/\partial z$, $w' = -\partial\psi/\partial x$, the buoyancy frequency $N^2 = -(g/\rho_0)(\mathrm{d}\bar{\rho}/\mathrm{d}z)$, and the Fourier structure $\exp[\mathrm{i}k(x-ct)]$ in the horizontal, we can reduce the problem to a single equation for ψ in terms of the remaining variable z:

$$(\bar{u}-c)\left(\frac{\mathrm{d}^2\psi}{\mathrm{d}z^2}-k^2\psi\right)+\left(\frac{N^2}{\bar{u}-c}-\frac{\mathrm{d}^2\bar{u}}{\mathrm{d}z^2}\right)\psi=0. \tag{14.10}$$

This is called the *Taylor–Goldstein equation* (Goldstein, 1931; Taylor, 1931). It governs the vertical structure of a perturbation in a stratified parallel flow. Note the formal analogy with the Rayleigh equation (10.9) governing the structure of a perturbation on a horizontally sheared flow in the absence of stratification and in the presence of rotation. Therefore, the same analysis can be applied.

First, we state the boundary conditions. For a domain bounded vertically by two horizontal planes, at $z=0$ and $z=H$, we impose a zero vertical velocity there, or, in terms of the streamfunction:

$$\psi(0)=\psi(H)=0. \tag{14.11}$$

Then, we recognize that the equation and its accompanying boundary conditions form an eigenvalue problem: Unless the phase velocity c takes on a particular value (eigenvalue), the solution is trivial ($\psi=0$). In general, the eigenvalues may be complex, but if c admits the function ψ, then its complex conjugate c^* admits the function ψ^* and is thus another eigenvalue. This can be easily verified by taking the complex conjugates of Eqs. (14.10) and (14.11). Hence, complex eigenvalues come in pairs. In each pair, one of the two eigenvalues will have a positive imaginary part and will correspond to an exponentially growing perturbation. The presence of a nonzero imaginary part to c automatically guarantees the existence of at least one unstable mode. Conversely, the basic flow is stable if and only if all possible phase speeds c are purely real.

Because it is impossible to solve problem (14.10) and (14.11) in the general case of an arbitrary shear flow $\bar{u}(z)$, we will limit ourselves, as in Section 10.2, to deriving integral constraints. A variety of such constraints can be established, but the most powerful one is obtained when the function ϕ, defined by

$$\psi=\sqrt{\bar{u}-c}\,\phi, \tag{14.12}$$

is used to replace ψ. Equation (14.10) and boundary conditions (14.11) become

$$\frac{\mathrm{d}}{\mathrm{d}z}\left[(\bar{u}-c)\frac{\mathrm{d}\phi}{\mathrm{d}z}\right]-\left[k^2(\bar{u}-c)+\frac{1}{2}\frac{\mathrm{d}^2\bar{u}}{\mathrm{d}z^2}+\frac{1}{\bar{u}-c}\left(\frac{1}{4}\left(\frac{\mathrm{d}\bar{u}}{\mathrm{d}z}\right)^2-N^2\right)\right]\phi=0 \tag{14.13}$$

$$\phi(0)=\phi(H)=0. \tag{14.14}$$

Multiplying Eq. (14.13) by the complex conjugate ϕ^*, integrating over the vertical extent of the domain, and utilizing conditions (14.14), we obtain

$$\int_0^H \left[N^2 - \frac{1}{4}\left(\frac{d\bar{u}}{dz}\right)^2 \right] \frac{|\phi|^2}{\bar{u}-c} dz = \int_0^H (\bar{u}-c)\left(\left|\frac{d\phi}{dz}\right|^2 + k^2|\phi|^2 \right) dz + \frac{1}{2}\int_0^H \frac{d^2\bar{u}}{dz^2}|\phi|^2 dz, \tag{14.15}$$

where vertical bars denote the absolute value of complex quantities. The imaginary part of this expression is

$$c_i \int_0^H \left[N^2 - \frac{1}{4}\left(\frac{d\bar{u}}{dz}\right)^2 \right] \frac{|\phi|^2}{|\bar{u}-c|^2} dz = -c_i \int_0^H \left(\left|\frac{d\phi}{dz}\right|^2 + k^2|\phi|^2 \right) dz, \tag{14.16}$$

where c_i is the imaginary part of c. If the flow is such that $N^2 > \frac{1}{4}(d\bar{u}/dz)^2$ everywhere, then the preceding equality requires that c_i times a positive quantity equals c_i times a negative quantity and, consequently, that c_i must be zero. This leads us to define the *Richardson number*

$$Ri = \frac{N^2}{(d\bar{u}/dz)^2} = \frac{N^2}{M^2}, \tag{14.17}$$

with $M = |d\bar{u}/dz|$ (called the Prandtl frequency), and the criterion is that if the inequality

$$Ri > \frac{1}{4} \tag{14.18}$$

holds everywhere in the domain, the stratified shear flow is stable.

Note that the criterion does not imply that c_i must be nonzero if the Richardson number falls below $1/4$ somewhere in the domain. Hence, inequality (14.18) is a sufficient condition for stability, whereas its converse is a necessary condition for instability. Atmospheric, oceanic, and laboratory data indicate, however, that the converse of (14.18) is generally a reliable predictor of instability.

If the shear flow is characterized by linear variations of velocity and density, with velocities and densities ranging from U_1 to U_2 and ρ_1 to ρ_2 ($\rho_2 > \rho_1$), respectively, over a depth H, then

$$M = \left|\frac{d\bar{u}}{dz}\right| = \frac{|U_1 - U_2|}{H}, \quad N^2 = -\frac{g}{\rho_0}\frac{d\rho}{dz} = \frac{g}{\rho_0}\frac{\rho_2 - \rho_1}{H},$$

and the Richardson criterion stated as the necessary condition for instability becomes

$$\frac{(\rho_2-\rho_1)gH}{\rho_0(U_1-U_2)^2} < \frac{1}{4}. \tag{14.19}$$

The similarity to Eq. (14.3) is not coincidental: Both conditions imply the possibility of large perturbations that could destroy the stratified shear flow. The difference in the numerical coefficients on the right-hand sides can be explained by the difference in the choice of the basic profile [discontinuous for Eq. (14.3), linear for Eq. (14.19)] and by the fact that the analysis leading to Eq. (14.3) did not make provision for a consumption of kinetic energy by vertical motions. The change from 1 in Eq. (14.3) to 1/4 in Eq. (14.19) is also consistent with the fact that condition (14.3) refers to complete mixing, whereas Eq. (14.19) is a condition for the onset of the instability.

More importantly, the similarity between Eqs. (14.3) and (14.19) imparts a physical meaning to the Richardson number: It is essentially a ratio between potential and kinetic energies, with the numerator being the potential-energy barrier that mixing must overcome if it is to occur and the denominator being the kinetic energy that the shear flow can supply when smoothed away. In fact, it was precisely by developing such energy considerations that British meteorologist Lewis Fry Richardson[2] first arrived, in 1920, to the dimensionless ratio that now rightfully bears his name. A first formal proof of criterion (14.18), however, did not come until four decades later (Miles, 1961).

In closing this section, it may be worth mentioning that bounds on the real and imaginary parts of the wave velocity c can be derived by inspection of certain integrals. This analysis, due to Louis N. Horward,[3] has already been applied to the study of barotropic instability (Section 10.3). Here, we summarize Howard's original derivation in the context of stratified shear flow. To begin, we introduce the vertical displacement a caused by the small wave perturbation, defined by

$$\frac{\partial a}{\partial t}+\bar{u}\frac{\partial a}{\partial x}=w$$

or

$$(\bar{u}-c)\,a=-\psi. \tag{14.20}$$

We then eliminate ψ from Eqs. (14.10) and (14.11) and obtain an equivalent problem for the variable a:

$$\frac{\mathrm{d}}{\mathrm{d}z}\left[(\bar{u}-c)^2\frac{\mathrm{d}a}{\mathrm{d}z}\right]+\left[N^2-k^2(\bar{u}-c)^2\right]a=0 \tag{14.21}$$

[2] See biography at the end of this chapter.
[3] See biography at end of Chapter 10.

$$a(0) = a(H) = 0. \tag{14.22}$$

A multiplication by the complex conjugate a^* followed by an integration over the domain and use of the boundary conditions yields

$$\int_0^H (\bar{u} - c)^2 P \, \mathrm{d}z = \int_0^H N^2 |a|^2 \mathrm{d}z, \tag{14.23}$$

where $P = |\mathrm{d}a/\mathrm{d}z|^2 + k^2|a|^2$ is a nonzero positive quantity. The imaginary part of this equation implies that if there is instability ($c_i \neq 0$), c_r must lie between the minimum and maximum values of $\bar{u}$, that is,

$$U_{\min} < c_r < U_{\max}. \tag{14.24}$$

Physically, the growing perturbation travels with the flow at some intermediate speed, and there exists at least one critical level in the domain where the perturbation is stationary with respect to the local flow. This local coupling between the wave and the flow is precisely what allows the wave to extract energy from the flow and to grow at its expense.

Now, the real part of Eq. (14.23),

$$\int_0^H \left[(\bar{u} - c_r)^2 - c_i^2 \right] P \mathrm{d}z = \int_0^H N^2 |a|^2 \mathrm{d}z \tag{14.25}$$

can be manipulated in a way similar to that used in Section 10.3 to obtain the following inequality:

$$\left(c_r - \frac{U_{\min} + U_{\max}}{2} \right)^2 + c_i^2 \leq \left(\frac{U_{\max} - U_{\min}}{2} \right)^2. \tag{14.26}$$

This implies that, in the complex plane, the number $c = c_r + \mathrm{i}c_i$ must lie within the circle that has the range $\bar{u}$ as diameter on the real axis. Because instability requires a positive imaginary value c_i, the interest is restricted to the upper half of the circle (Fig. 10.1). This result is called the Howard semicircle theorem. In particular, it implies that c_i is bounded by $(U_{\max} - U_{\min})/2$, providing a useful upper bound on the growth rate of unstable perturbations:

$$kc_i \leq \frac{k}{2} (U_{\max} - U_{\min}). \tag{14.27}$$

14.3 TURBULENCE CLOSURE: k-MODELS

Reynolds averaging (Section 4.1) showed that small-scale processes, as those involved during turbulence and mixing, affect the mean flow through the so-called Reynolds stresses, which stem from the nonlinear advection terms

in the momentum equations. Till now, Reynolds stresses were represented as diffusive fluxes and thus modeled with the help of an eddy viscosity. What value should be assigned to this eddy viscosity was not said. The fact is that setting a value to this parameter is far from trivial because it does not represent a unique fluid property, such as molecular viscosity, but rather reflects the level of turbulence in the particular flow under consideration. The value of the eddy viscosity should therefore not be expected to be a constant but ought to depend on characteristics of the flow conditions at the time and place of consideration. All we can hope for is that the local level of turbulence can be related to flow properties on the larger, resolved scale. Put another way, the determination of the eddy viscosity is in fact part of the problem. This forces us to consider how fluctuations actually behave.

A naive approach consists of calculating fluctuations such as u' by taking the original, nonaveraged equation for u and subtracting its Reynolds average (4.4) in order to obtain an equation for the fluctuation u', and similarly for the other variables. In principle, solving these "perturbation equations" should allow us to determine the fluctuations (such as u' and w'), from which we can then form products and obtain the Reynolds averages (such as $\langle u'w' \rangle$). This process, unfortunately, is not working.

To illustrate the nature of the problem, let us simplify the notation by introducing $\mathcal{L}$, an arbitrary linear operator, and start from a much reduced equation with quadratic nonlinearity of the type

$$\frac{\partial u}{\partial t} + \mathcal{L}(uu) = 0. \tag{14.28}$$

Its Reynolds average (see Section 4.1) is

$$\frac{\partial \langle u \rangle}{\partial t} + \mathcal{L}(\langle u \rangle \langle u \rangle) + \mathcal{L}\left(\langle u'u' \rangle\right) = 0, \tag{14.29}$$

from which we can obtain the equation governing the fluctuation u' by subtraction:

$$\frac{\partial u'}{\partial t} + 2\mathcal{L}\left(\langle u \rangle u'\right) + \mathcal{L}\left(u'u'\right) - \mathcal{L}\left(\langle u'u' \rangle\right) = 0. \tag{14.30}$$

Solving this equation should provide u' and allow us to calculate the Reynolds stress $\langle u'u' \rangle$, but it is clearly not realistic since we initially set out to separate the fluctuation so that we would not have to solve for it. What we want is only the average of a certain product and none of the details. With this in mind, let us start from the equation for the fluctuation (and not its solution) and seek an equation governing directly the desired average. To do so, we multiply

Eq. (14.30) by the fluctuation and then take the average of the product.[4] This yields a predictive equation for the desired quantity $\langle u'u' \rangle$:

$$\frac{1}{2}\frac{\partial \langle u'u' \rangle}{\partial t} + 2\langle u' \mathcal{L}\left(\langle u \rangle u' \right) \rangle + \langle u' \mathcal{L}\left(u'u' \right) \rangle = 0, \tag{14.31}$$

in which we used $\langle u' \rangle = 0$ because a fluctuation has no average by definition.

From the last term of Eq. (14.31) emerges an annoying triple correlation, which no equation so far can provide. Should we try to establish a governing equation for this triplet (or third-order moment) by persevering with the same approach, it comes as no surprise that a fourth-order term arises, and so on endlessly. This means that we face a *closure problem*, and at some level of the process, we need to parameterize the unknown higher-order products in terms of those of lower order in a way that remains faithful to the physical phenomenology of turbulence and keeps modeling errors small.

It is generally accepted, more by intuition than by proof, that the higher the order at which truncation is performed and parameterization introduced, the lesser the modeling error. Stopping at second-order correlations is done almost universally in the context of field data and laboratory experiments (e.g., Gibson & Launder, 1978; Pope, 2000). The attending models are full *second-order closure* or *second-moment closure* schemes that calculate all Reynolds stresses involving products of variables by means of evolution equations relying on closure assumptions at the level of third-order correlations.

Here we restrict our attention to the two simplest versions of second-order schemes, in which only some of the second moments are determined by their evolution equations, whereas the others are governed by simpler equations containing no time derivative (so-called *diagnostic equations*). Such models continue to be called second-order closure schemes and are distinguished by explicitly naming the higher-order moments that are parameterized. An example is the k *model* that is presented below.

We begin by identifying key features of turbulence from which we can establish a practical closure scheme. The most obvious property of a turbulent flow is its ability to mix the fluid efficiently. This is why we stir our *café au lait* rather than wait for molecular diffusion to distribute the milk evenly across the black coffee. Turbulence-enhanced mixing is the reason why Reynolds stresses are most often expressed as diffusion terms. Shear in the mean flow generates instabilities, which are manifested by eddies at many scales. The larger eddies reflect the anisotropy of the mean flow, but rapid fluctuations at the shorter scales

[4]Here we assume that the averaging operation commutes with time and space derivatives. Also, the average of an average is the first average. Should our average not be an average over multiple realizations (so-called *ensemble average*) but rather an average over time or space, it is necessary that the temporal or spatial scales of the fluctuation be clearly separated from that of the mean flow (e.g., Burchard, 2002).

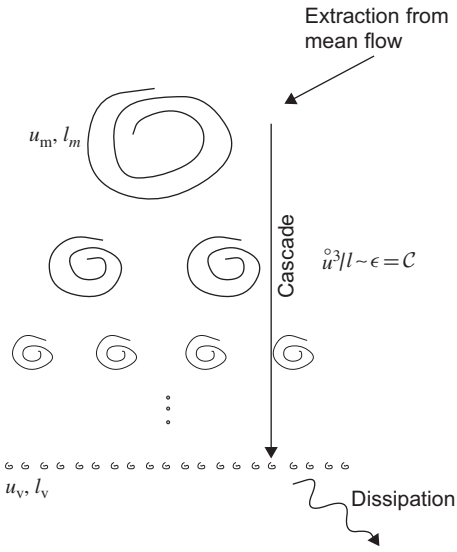

FIGURE 14.7 The oft-quoted lines of Lewis Fry Richardson "*the big whirls have little whirls that feed on their velocities, and little whirls have lesser whirls and so on to viscosity – in the molecular sense*" taken from his 1922 book aptly summarizes the idea used in turbulence modeling according to which turbulence effects a gradual transfer of energy from the broader and unstable flow to the smallest eddies that dissipate it.

appear erratic and isotropic. There is, however, no clear distinction between the two types of fluctuations, only a broad transition called the *energy cascade* (Kolmogorov, 1941; Fig. 14.7). For eddies of velocity scale $\mathring{u}$ and diameter d within the cascade, the Reynolds number is very large so that their evolution is fast compared with the decay time due to viscosity. Nonlinear advection is therefore dominant, rapidly breaking the eddies down into smaller ones. The energy continuously extracted from the mean flow by its instabilities is thus transferred gradually from the larger eddies to the smaller ones without appreciable loss to viscosity. This energy is eventually dissipated at the shortest scales. Because of the lack of dissipation through the cascade, the dissipation rate is thus conserved across the cascade. Since viscosity does not influence the dissipation rate within the cascade, the only parameters that can be related to the dissipation rate denoted as ϵ are the velocity scale $\mathring{u}$ and length scale d of the eddies, the time scale being determined by the turnover scale $d/\mathring{u}$, hence $\epsilon = \epsilon(\mathring{u}, d)$. The dimensionally correct relation is

$$\epsilon = \left(\frac{c_\mu^0}{4}\right)^{3/4} \frac{\mathring{u}^3}{d}, \tag{14.32}$$

in which we introduced a calibration constant $c_\mu^0 \sim 0.1$ in a combination that will be useful later. We recover the result of Section 5.1. Also the value of ϵ is the one that is extracted from the mean flow at velocity scale u_m and length scale l_m, called *macro scales* and $\epsilon = \epsilon(\mathring{u}, d) = \epsilon(u_\mathrm{m}, l_m)$.

Relation (14.32) shows that for a given turbulence cascade, $\mathring{u} \propto d^{1/3}$, stating that the smaller eddies contain less kinetic energy than the larger ones, so that the bulk of kinetic energy is attributable to the largest eddies of size l_m (Fig. 14.7). The kinetic-energy spectrum must therefore be decreasing with increasing wavenumber according to Eq. (5.8) of Section 5.1. The turbulent cascade may also be interpreted in terms of vorticity. In three dimensions, vortex tubes are twisted and stretched by other, adjacent or containing vortex tubes (in a manner similar to the two-dimensional straining encountered in Fig. 10.12), and because of incompressibility, stretching in one direction is accompanied by squeezing in another, and conservation of circulation demands an increase in vorticity. Vorticity, therefore, is increasing with decreasing eddy length scale.

The cascade cannot, of course, continue down to arbitrarily small scales, and at some small but finite scale, molecular viscosity comes into play. The scale l_v at which this occurs is the one for which viscous friction becomes a dominant term in the momentum equation, that is, the scale that renders the Reynolds number, ratio of inertia to friction, of order unity:

$$\frac{u\partial u/\partial x}{\nu\ \partial^2 u/\partial x^2} \sim \frac{u_\mathrm{v}^2/l_\mathrm{v}}{\nu u_\mathrm{v}/l_\mathrm{v}^2} = \mathcal{O}(1). \tag{14.33}$$

The length and velocity scales, l_v and u_v, at which this *viscous sink* occurs are called *micro scales* or *viscous scales*. The preceding equation implies that they are linked by the following relation:

$$\frac{u_\mathrm{v} l_\mathrm{v}}{\nu} \sim 1. \tag{14.34}$$

Since Eq. (14.32) continues to hold down to that scale, we also have

$$\epsilon \propto \frac{u_\mathrm{v}^3}{l_\mathrm{v}} = \frac{u_\mathrm{m}^3}{l_m}, \tag{14.35}$$

and we can determine the range of scales in the eddy cascade by eliminating u_v between Eqs. (14.35) and (14.34) and by expressing u_m in terms of the Reynolds number $u_\mathrm{m} l_m/\nu$ of the macroscale:

$$\frac{l_m}{l_\mathrm{v}} \sim Re^{3/4}. \tag{14.36}$$

High Reynolds-number flows, therefore, are characterized by broad eddy cascades.

Alternatively, we can express the scales at which dissipation takes place as functions of the dissipation rate and molecular viscosity by eliminating u_v from Eqs. (14.32) and (14.34):

$$l_\mathrm{v} \sim \epsilon^{-1/4} \nu^{3/4}. \tag{14.37}$$

Thus, the more energy is fed into turbulence by the mean flow, the smaller the ultimate eddies are in order to dissipate that energy. Or, back to a more familiar situation, the more strongly we stir our coffee, the smaller the eddies, and the more efficient the mixing. It is worth insisting that it is molecular viscosity that is ultimately responsible for the diffusion. The turbulent cascade simply increases the shearing and tearing on fluid parcels, increasing contact between initially separated fluid parcels and increasing spatial gradients so that molecular diffusion can act more efficiently (Fig. 14.8).

Integrating the energy spectrum Eq. (5.8) from the longest to the shortest eddy sizes yields the total kinetic energy of the inertial range:

$$\int_{\pi/l_m}^{\pi/l_v} E_k \mathrm{d}k = \frac{u_m^2}{2}\left(1 - \frac{1}{\sqrt{Re}}\right) \sim \frac{u_m^2}{2}, \tag{14.38}$$

and hence the total turbulent kinetic energy in the flow does not differ much from that of the largest eddies.

Having now some idea on how energy is extracted from the mean flow, we can return to the challenge of representing the effect of this cascade in a model via an eddy viscosity. We limit our search to a parameterization in which the properties of the turbulent cascade are purely local (so-called *one-point closure model*) and do not involve remote parameters. For the mean flow, we suppose that l_m is the scale at which turbulence extracts energy, and since we do not resolve the cascade and its associated velocity fluctuations u' explicitly, the dissipation introduced by the eddy viscosity must extract the ϵ energy per time.

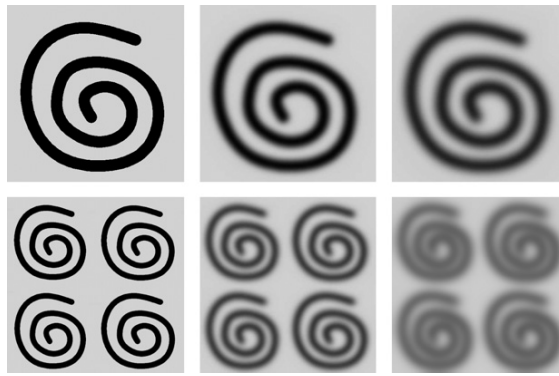

FIGURE 14.8 Effect of eddy size on diffusion over time. With time increasing from left to right, the top row illustrates the progressive action of diffusion on a structure of larger scale, whereas the bottom row shows that on a structure of shorter size. Note how diffusion acts more effectively at the shorter scale. For the same molecular diffusivity, mixing occurs more effectively at shorter scales because regions of different properties are in closer contact. (*Figure prepared at the suggestion of Hans Burchard*)

To accomplish this, the Reynolds number based on the eddy viscosity must be on the order of unity at the level of l_m:

$$\frac{u_{\mathrm{m}} l_m}{\nu_{\mathrm{E}}} \sim 1. \tag{14.39}$$

The eddy viscosity concept ensures that fluid parcels moving with the eddy velocity u_{m} over the distance l_m exchange momentum with other fluids parcels, as in molecular diffusion where momentum exchange between molecules occurs over the mean free path. Within this context, it is not surprising that the term *mixing length* was coined for l_m.

With Eq. (14.39), we ensure that some energy is extracted from the mean flow using an eddy viscosity approach. That this amount of energy extraction per unit time be equal to ϵ is an additional requirement. Assuming we know this dissipation rate, we require

$$\frac{u_{\mathrm{m}}^3}{l_m} = \frac{\epsilon}{(c_\mu^0/4)^{3/4}}. \tag{14.40}$$

In summary, the formulation of the eddy viscosity demands that we know the scales u_{m} and l_m. If we also know the dissipation rate ϵ, we can use Eq. (14.40) to reduce the number of scales to be prescribed. If in addition, we know the kinetic energy k at the macroscale, this would add another relation that determines the velocity scale:

$$\mathsf{k} = \frac{u_{\mathrm{m}}^2}{2}. \tag{14.41}$$

This can also be used to calculate the dissipation rate (14.40) as follows:

$$\epsilon = \left(c_\mu^0\right)^{3/4} \frac{\mathsf{k}^{3/2}}{l_m}. \tag{14.42}$$

Knowing k and ϵ would thus allow the calculation of the eddy viscosity ν_{E} and complete our closure scheme. At this point, the reader might object that calculating a macroscale length using a microscale dissipation rate sounds contradictory, but the paradox is easily explained by the fact that in the Kolmogorov theory, the dissipation rate at the microscale is equal to the energy input at the macroscale, hence the link. This justification and most of the previous reasoning rely on the idea of a statistical equilibrium state of turbulence in which, at each moment, energy input in the mean flow matches energy removal at the shortest scales.

One of the first successful attempts to quantify the eddy viscosity by means of a velocity and length scale is credited to Ludwig Prandtl[5] who considered

[5] See biography at the end of Chapter 8.

a vertically sheared horizontal flow $\langle u \rangle(z)$ and assumed the velocity fluctuations to be statistically random except for a nonzero correlation between the horizontal and vertical velocity fluctuations, u' and w'. In such a case,

$$\langle u'w' \rangle = r \sqrt{\langle u'^2 \rangle} \sqrt{\langle w'^2 \rangle}, \tag{14.43}$$

where r is the correlation coefficient between u' and w'. Assuming that each velocity fluctuation is proportional to the velocity scale u_m of the coherent structures causing the correlation, we can write

$$\langle u'w' \rangle = c_1 u_\mathrm{m}^2 \tag{14.44}$$

with a constant coefficient of proportionality c_1. Since the eddy viscosity is defined from

$$\langle u'w' \rangle = -\nu_\mathrm{E} \frac{\partial \langle u \rangle}{\partial z}, \qquad \nu_\mathrm{E} = u_\mathrm{m} l_m, \tag{14.45}$$

we obtain an expression for the eddy viscosity that depends only on mean flow quantities, thus yielding a first turbulence-closure model:

$$u_\mathrm{m} = l_m \left| \frac{\partial \langle u \rangle}{\partial z} \right| \quad \text{and} \quad \nu_\mathrm{E} = l_m^2 \left| \frac{\partial \langle u \rangle}{\partial z} \right|, \tag{14.46}$$

Here, the absolute value is introduced to ensure a positive value for the eddy viscosity. We note that this model predicts increasing turbulent diffusion under increased shear, in accordance with our intuition that shear is destabilizing and the cause of turbulence.

The only remaining parameter that Prandtl needed to determine was the mixing length, in which all calibration constants come together. The determination of the mixing length depends on the particular situation, especially its geometry. For example, a flow along a rigid boundary is characterized by an eddy size increasing with distance from the boundary, and thus a larger l_m at a greater distance from the boundary.

Because $\langle u'w' \rangle$ must vanish at a rigid boundary, so must the Reynolds stress. Since it is now expressed as $-l_m^2 |\partial \langle u \rangle / \partial z|^2$ with the present closure scheme, it is clear that the mixing length, too, must go to zero at the boundary. As a result, the mixing length in the vicinity of a solid boundary is often expressed as $l_m = \mathcal{K} z$, in which z is the distance from the boundary and $\mathcal{K}$ the so-called *von Kármán constant* (e.g., Nezu & Nakagawa, 1993; see also Section 8.1).

The preceding closure scheme relying on the concept of a mixing length l_m may be modified in order to accommodate the stabilizing effect of stratification and also generalized to three dimensions. These modifications will be explored later when we show that the Prandtl model can be seen as a simplification of more complex turbulence closure schemes. Despite the advantage of its algebraic nature, which is easily implemented, Prandtl's scheme suffers from

the fact that it assumes a turbulence level determined solely by the instantaneous flow. No memory effect is included, and as soon as mixing eradicates the shear, the eddy viscosity falls to zero, whereas in reality, turbulence never stops abruptly but undergoes gradual decay. This is one among several problems of a so-called *zero-equation turbulence model*. Clearly, more sophisticated schemes are often necessary.

To develop models with memory effect, we seek governing equations with time derivatives (*prognostic equations* as opposed to *diagnostic equations*) for some of the second moments. First, we note that the difference between volume conservation of the total flow, Eq. (3.17), and of the mean flow only, Eq. (4.9), provides a constraint on the velocity fluctuations:

$$\frac{\partial u'}{\partial x}+\frac{\partial v'}{\partial y}+\frac{\partial w'}{\partial z}=0. \tag{14.47}$$

We can then use this constraint in our manipulation of the governing equations for the Reynolds stresses. The two most natural candidates for diagnostic equations are those for the turbulent kinetic energy k and dissipation rate ϵ because they together capture the primary characteristics of the turbulent environment. Their values also set the scales in formulating the eddy viscosity.

Here, we start by developing the so-called turbulent kinetic energy model in which k is defined[6] as

$$\mathsf{k}=\frac{\langle u'^2\rangle+\langle v'^2\rangle+\langle w'^2\rangle}{2}. \tag{14.48}$$

In view of Eqs. (14.32) and (14.38), the bulk of the turbulent kinetic energy is contained in the largest eddies so that we may use the velocity scale of the largest eddies as $\sqrt{2\mathsf{k}}$. We are then in a position of establishing a governing equation for k by applying a closure approach.

Taking the difference between Eqs. (3.19) and (4.7a), we obtain the evolution equation for the fluctuation u', which we then multiply by u' itself. Doing the same with the equations for v' and w', and adding the three together, we obtain after some tedious algebra and the use of Eq. (14.47) the following evolution equation for k:

$$\frac{\mathrm{d}\mathsf{k}}{\mathrm{d}t}=P_s+P_b-\epsilon-\left(\frac{\partial q_x}{\partial x}+\frac{\partial q_y}{\partial y}+\frac{\partial q_z}{\partial z}\right), \tag{14.49}$$

in which we arranged the various terms for a better understanding of the physics. First, the time derivative is the material derivative based on the mean flow,

[6]To be exact, k is the turbulent kinetic energy per unit of mass of fluid. By virtue of the Boussinesq approximation, however, the ratio between energy and energy per mass is the reference density ρ_0, which is a constant.

namely,

$$\frac{\mathrm{d}}{\mathrm{d}t} = \frac{\partial}{\partial t} + \langle u \rangle \frac{\partial}{\partial x} + \langle v \rangle \frac{\partial}{\partial y} + \langle w \rangle \frac{\partial}{\partial z},$$

and we note that the Coriolis terms have canceled one another out, which is not too surprising since the Coriolis force does not perform mechanical work and should therefore not affect a kinetic energy budget.

With no approximation invoked, the other terms[7] are

$$\begin{aligned} P_s = &-\langle u'u' \rangle \frac{\partial \langle u \rangle}{\partial x} - \langle u'v' \rangle \frac{\partial \langle u \rangle}{\partial y} - \langle u'w' \rangle \frac{\partial \langle u \rangle}{\partial z} \\ &-\langle v'u' \rangle \frac{\partial \langle v \rangle}{\partial x} - \langle v'v' \rangle \frac{\partial \langle v \rangle}{\partial y} - \langle v'w' \rangle \frac{\partial \langle v \rangle}{\partial z} \\ &-\langle w'u' \rangle \frac{\partial \langle w \rangle}{\partial x} - \langle w'v' \rangle \frac{\partial \langle w \rangle}{\partial y} - \langle w'w' \rangle \frac{\partial \langle w \rangle}{\partial z} \end{aligned} \tag{14.50}$$

$$P_b = -\langle \rho' w' \rangle \frac{g}{\rho_0} \tag{14.51}$$

$$\begin{aligned} \frac{\epsilon}{\nu} = &\left\langle \frac{\partial u'}{\partial x} \frac{\partial u'}{\partial x} \right\rangle + \left\langle \frac{\partial u'}{\partial y} \frac{\partial u'}{\partial y} \right\rangle + \left\langle \frac{\partial u'}{\partial z} \frac{\partial u'}{\partial z} \right\rangle \\ &+ \left\langle \frac{\partial v'}{\partial x} \frac{\partial v'}{\partial x} \right\rangle + \left\langle \frac{\partial v'}{\partial y} \frac{\partial v'}{\partial y} \right\rangle + \left\langle \frac{\partial v'}{\partial z} \frac{\partial v'}{\partial z} \right\rangle \\ &+ \left\langle \frac{\partial w'}{\partial x} \frac{\partial w'}{\partial x} \right\rangle + \left\langle \frac{\partial w'}{\partial y} \frac{\partial w'}{\partial y} \right\rangle + \left\langle \frac{\partial w'}{\partial z} \frac{\partial w'}{\partial z} \right\rangle \end{aligned} \tag{14.52}$$

$$q_x = \frac{1}{\rho} \left\langle \left(p' + \frac{u'^2 + v'^2 + w'^2}{2} \right) u' \right\rangle - \nu \frac{\partial \mathrm{k}}{\partial x} \tag{14.53}$$

and similar expressions for q_y and q_z. All terms involve unknown averages for which we now need to make closure assumptions.

Because the quantity P_s involves both mean flow and turbulence, it stems from the interaction between the two. The presence of the shear of the large-scale flow suggests that we call it *shear production*. The second term, P_b, clearly involves the work performed by the turbulent buoyancy forces on the vertical stratification and is thus related to potential-energy changes. For obvious reasons we call it *buoyancy production*. The dissipation rate ϵ involves, as expected, the molecular viscous dissipation by turbulent motions. Finally, the vector (q_x, q_y, q_z) involves only turbulent fluctuations of pressure and velocity, and its divergence form in the turbulent kinetic energy budget (14.49) indicates

[7] Strictly speaking, the dissipation term should be $\epsilon = 2\nu \|\mathbf{D}\|^2$ in which the deformation tensor $\mathbf{D}$ of the fluctuations is similar to Eq. (14.54). The definition used here is often called pseudo dissipation.

that it represents a spatial redistribution of k by turbulence, not contributing to production or dissipation.

All those terms must now be modeled in terms of the state variables. For example, the Reynolds stresses appearing in the unknown terms are replaced by the eddy-viscosity parameterization already shown. By defining the deformation tensor (or strain-rate tensor)

$$\mathbf{D}=\frac{1}{2}\begin{pmatrix} 2\frac{\partial u}{\partial x} & \left(\frac{\partial u}{\partial y}+\frac{\partial v}{\partial x}\right) & \left(\frac{\partial u}{\partial z}+\frac{\partial w}{\partial x}\right) \\ \left(\frac{\partial u}{\partial y}+\frac{\partial v}{\partial x}\right) & 2\frac{\partial v}{\partial y} & \left(\frac{\partial v}{\partial z}+\frac{\partial w}{\partial y}\right) \\ \left(\frac{\partial u}{\partial z}+\frac{\partial w}{\partial y}\right) & \left(\frac{\partial v}{\partial z}+\frac{\partial w}{\partial x}\right) & 2\frac{\partial w}{\partial z} \end{pmatrix} \tag{14.54}$$

and the Reynolds stress tensor

$$\boldsymbol{\tau}=\begin{pmatrix} \langle u'u'\rangle & \langle u'v'\rangle & \langle u'w'\rangle \\ \langle u'v'\rangle & \langle v'v'\rangle & \langle v'w'\rangle \\ \langle u'w'\rangle & \langle v'w'\rangle & \langle w'w'\rangle \end{pmatrix}, \tag{14.55}$$

the eddy-viscosity model is

$$\boldsymbol{\tau}=-2\nu_{\mathrm{E}}\mathbf{D}+\frac{2\mathrm{k}}{3}\mathbf{I}. \tag{14.56}$$

The first term on the right-hand side is a familiar expression relating the (turbulent) stress to the rate of strain. The appearance of the second term, proportional to k and involving the identity matrix **I**, begs for an explanation. Without it the parameterization is faulty: The trace of the stress tensor on the left-hand side must be equal to the trace on the right-hand side, and this constraint justifies the presence of the second term. In practice, this term is not a dominant one, but it is readily calculated with a k model. Using Eq. (14.56) in Eq. (14.50) expresses the shear production P_s in terms of the mean-flow characteristics.

For the buoyancy production term, P_b, the velocity-density correlations are modeled with the help of the eddy-diffusivity approach

$$\langle\rho'w'\rangle=-\kappa_{\mathrm{E}}\frac{\partial\langle\rho\rangle}{\partial z}=\kappa_{\mathrm{E}}\frac{\rho_0}{g}N^2 \tag{14.57}$$

in which κ_{E} is a turbulent diffusivity that is part of the closure scheme. Aside from the latter, the term P_b does not require any further treatment.

Since the flux terms q_x, q_y, and q_z appear in divergence form in Eq. (14.49), they are only responsible for redistributing k in space. This is coupled to the fact that they involve turbulent quantities, suggesting that we model these terms as turbulent diffusion of k. In view of the velocity and pressure correlations

involved,[8] the eddy viscosity ν_E is used for the flux calculation rather than the eddy diffusivity κ_E.

In summary, the various terms are parameterized as follows:

$$P_s = 2\nu_E \| \langle \mathbf{D} \rangle \| \tag{14.58}$$

$$P_b = -\kappa_E N^2 \tag{14.59}$$

$$q_x = -\nu_E \frac{\partial \mathrm{k}}{\partial x} \quad q_y = -\nu_E \frac{\partial \mathrm{k}}{\partial y} \quad q_z = -\nu_E \frac{\partial \mathrm{k}}{\partial z}. \tag{14.60}$$

We notice that the sign of the modeled term P_s is consistent with the idea of turbulence extracting energy from the mean flow and transferring it to turbulence. Similarly, the sign of P_b indicates that stratification inhibits turbulence because of the increase of potential energy required by mixing a stably stratified system (Section 14.2).

With these parameterizations, Eq. (14.49) governing the evolution of turbulent kinetic energy becomes

$$\frac{\mathrm{dk}}{\mathrm{d}t} = P_s + P_b - \epsilon + \mathcal{D}(\mathrm{k}), \tag{14.61}$$

$$\mathcal{D}(\mathrm{k}) = \frac{\partial}{\partial z}\left(\nu_E \frac{\partial \mathrm{k}}{\partial z}\right). \tag{14.62}$$

Note that the turbulent diffusion has been reduced to its the vertical component. The horizontal part is awaiting a subsequent parameterization of horizontal subgrid scales.

With appropriate boundary conditions, we can predict the evolution of k if we know how to calculate ϵ, the eddy viscosity ν_E, and the eddy diffusivity κ_E. With ϵ calculated using Eq. (14.42) and mixing length l_m prescribed, the turbulent closure scheme is called a k-model or *one-equation turbulence model*. The energy of the turbulent eddies gives a reliable estimate of their velocity and hence of the eddy viscosity via

$$\nu_E = \frac{c_\mu}{\left(c_\mu^0\right)^{3/4}} \sqrt{\mathrm{k}}\, l_m. \tag{14.63}$$

Note that in this scheme, the mixing length must be prescribed independently. This is usually done based on geometrical considerations of the flow. The value of ϵ is then obtained from Eq. (14.35) for use in Eq. (14.61) to predict k. The constant c_μ^0 is the same constant as in Eq. (14.42), whereas c_μ is a calibration parameter.

[8] In state-of-the art models, the eddy diffusivity for turbulent kinetic energy is the eddy diffusivity divided by the so-called *Schmidt number*.

The eddy diffusivity κ_E is obtained in a similar way:

$$\kappa_E = \frac{c'_\mu}{\left(c^0_\mu\right)^{3/4}} \sqrt{\mathrm{k}}\, l_m, \tag{14.64}$$

where the calibration constant c'_μ differs from c_μ. The two parameters will be defined later as functions of shear and stratification.

For simplicity, we introduced only two different turbulent-diffusion coefficients, although each state variable could claim its own (e.g., Canuto, Howard, Cheng & Dubovikov, 2001). We utilize a unique κ_E for diffusion of all scalar fields because they are subjected to the same turbulent transport. Hence κ_E is used for the diffusion of density, salinity, temperature, moisture, or any other tracer concentration. In contrast, the eddy viscosity ν_E is used for the diffusion of momentum, k and ϵ, the dynamical variables.

Before exploring more advanced closure schemes, we can verify how the present model performs in a simple flow situation, such as a vertically sheared flow of uniform density. We align the x-axis with the mean flow and the z-axis with the shear. In this way, averaged fields are independent of x and y (Fig. 14.9), and the velocity field is simply $u = \langle u \rangle + u'$, $w = w'$. The mean flow depends only on z and obeys

$$\frac{\partial \langle u \rangle}{\partial t} = -\frac{1}{\rho_0}\frac{\partial \langle p \rangle}{\partial x} + \frac{\partial}{\partial z}\left(\nu \frac{\partial \langle u \rangle}{\partial z} - \langle u'w' \rangle\right). \tag{14.65}$$

The pressure gradient is uniform, and over a distance L along the x-axis, the pressure difference is $p_2 - p_1$. The kinetic energy $KE = \langle (u^2 + v^2 + w^2) \rangle / 2$ of the flow can be split into mean and turbulent contributions:

$$KE = \frac{\langle u \rangle^2}{2} + \mathrm{k}. \tag{14.66}$$

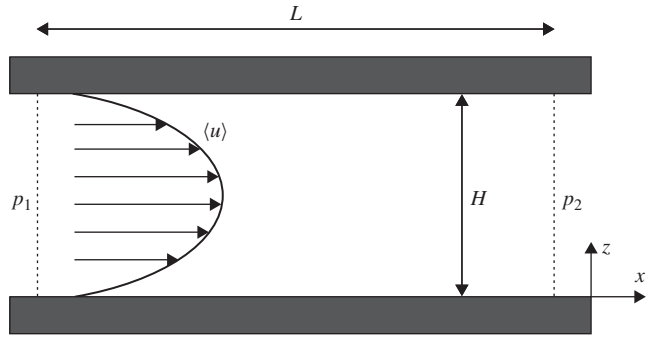

FIGURE 14.9 Flow between two horizontal planes forced by an external pressure gradient.

Multiplying Eq. (14.65) by $\langle u\rangle$, we can construct the governing equation for the kinetic energy of the mean flow. For the turbulent part, we can perform the same manipulation on the equations governing the fluctuations (not written down). With the simplifications pertinent to the present flow, the outcome is

$$\frac{\partial}{\partial t}\frac{\langle u\rangle^2}{2} = -\frac{1}{\rho_0}\frac{\partial \langle p\rangle \langle u\rangle}{\partial x} + \frac{\partial}{\partial z}\left[\langle u\rangle\left(\nu\frac{\partial \langle u\rangle}{\partial z} - \langle u'w'\rangle\right)\right] - \nu\left(\frac{\partial \langle u\rangle}{\partial z}\right)^2 + \underline{\langle u'w'\rangle\frac{\partial \langle u\rangle}{\partial z}}$$

$$\frac{\partial \mathrm{k}}{\partial t} = \underline{-\langle u'w'\rangle\frac{\partial \langle u\rangle}{\partial z}} - \epsilon + \frac{\partial q_z}{\partial z}. \tag{14.67}$$

The underlined term in the second equation is identified as the shear production of turbulence, and we note that it also appears in the first equation with opposite sign. Clearly, the shear production of turbulence is at the expense of mean-flow energy.

With the eddy-viscosity approach outlined earlier, the shear production term is expressed as

$$P_s = -\langle u'w'\rangle\frac{\partial \langle u\rangle}{\partial z} = \nu_{\mathrm{E}}\left(\frac{\partial \langle u\rangle}{\partial z}\right)^2. \tag{14.68}$$

For positive eddy viscosity, energy is extracted from the mean flow and feeds the turbulence.

If we integrate both energy equations over a distance L and across the domain height, assume steady state (for averages), exploit the fact that the velocities (both mean and turbulent) are zero at bottom ($z=0$) and top ($z=H$), and finally use the closure scheme, we obtain

$$\left(\frac{p_1-p_2}{\rho_0}\right)\frac{UH}{L} = \int_0^H (\nu_{\mathrm{E}}+\nu)\left(\frac{\partial \langle u\rangle}{\partial z}\right)^2 \mathrm{d}z \tag{14.69}$$

in which $U=(1/H)\int_0^H \langle u\rangle\,\mathrm{d}z$ is the average velocity over the inflow and outflow sections. For the turbulent kinetic energy, we have a similar budget

$$\int_0^H \epsilon\,\mathrm{d}z = \int_0^H \nu_{\mathrm{E}}\left(\frac{\partial \langle u\rangle}{\partial z}\right)^2 \mathrm{d}z. \tag{14.70}$$

Let us now interpret these budgets. In the absence of turbulence, eddy viscosity is zero, and the energy equation (14.69) for the mean flow then shows that for an increased energy input by a higher pressure gradient, the flow must generate increasing shear so that molecular viscosity can dissipate this energy.

However, when shear increases, the flow is prone to instabilities and eventually becomes turbulent. We see that energy is now extracted from the mean flow at much lower values of the shear because of the presence of $\nu_E \gg \nu$ in the right-hand side. The energy budget (14.70) for the turbulence confirms that the energy extracted from the mean flow is dissipated in the viscous sink by ϵ. We verify that molecular viscosity remains the ultimate sink of energy but at the much shorter scales of turbulence.

14.4 OTHER CLOSURES: $\mathsf{k}-\epsilon$ AND $\mathsf{k}-\mathsf{k}l_m$

To form a closed system of equations, the previous one-equation turbulence model needed the mixing length to be prescribed a priori. To avoid this, it is desirable to move from one governing equation (for k) to two governing equations (for k and l_m, or for k and ϵ). It is therefore no surprise to find a vast literature proposing governing equations for a combination of k and l_m, or equivalently a combination of k and ϵ. From the two calculated quantities, the third can always be determined from the algebraic relationship (14.42) and then the eddy viscosity via Eq. (14.63) or similar expression.

Since dissipation rates can be measured in the ocean by microprofilers (e.g., Lueck, Wolk & Yamazaki, 2002; Osborn, 1974), ϵ is an attractive candidate for a second equation in turbulence modeling. By manipulating the governing equations for velocity fluctuations in a similar way as for k, we can formulate a governing equation for ϵ of the type

$$\frac{\mathrm{d}\epsilon}{\mathrm{d}t} = Q, \tag{14.71}$$

in which the right-hand side contains a series of complicated expressions involving higher-order correlations (e.g., Burchard, 2002; Rodi, 1980). Unlike the k equation, however, these terms cannot be systematically modeled using the eddy-viscosity approach, and additional hypotheses, not to say educated guesses, are required. The most common approach is to use from the k equation the terms related to energy production and use them in linear combinations to close the energy dissipation source terms. Terms related to spatial redistribution of energy are, as usual, modeled by a turbulent diffusion. When all is said and done, the governing equation for ϵ is expressed as

$$\frac{\mathrm{d}\epsilon}{\mathrm{d}t} = \frac{\epsilon}{\mathsf{k}}\left(c_1 P_s + c_3 P_b - c_2 \epsilon\right) + \mathcal{D}(\epsilon), \tag{14.72}$$

where the terms P_s and P_b are the same as in the k equation and the coefficients c_1, c_2, and c_3 are calibration constants: $c_1 \approx 1.44$, $c_2 \approx 1.92$, $-0.6 \lesssim c_3 \lesssim 0.3$. Because the two turbulent quantities that are calculated in this model are k and ϵ, it is useful to express the eddy viscosity as a function of these by eliminating

the mixing length l_m between Eqs. (14.63) and (14.42) to obtain

$$\nu_{\mathrm{E}} = c_\mu \frac{\mathrm{k}^2}{\epsilon}. \tag{14.73}$$

This outlines a particular *two-equation turbulence model* within an array of possible other ones. Instead of formulating the governing equation for ϵ, an equation for l_m or a combination of l_m and k can also be established, with Eq. (14.42) providing a link between the three variables k, ϵ, and l_m.

A very popular scheme in the context of geophysical flows is the so-called $\mathrm{k}-\mathrm{k}l_m$ model of Mellor and Yamada (1982), of which the governing equation for $\mathrm{k}l_m$ is

$$\frac{\mathrm{d}\mathrm{k}l_m}{\mathrm{d}t} = \frac{l_m}{2}\left[E_1 P_s + E_3 P_b - \left(1 - E_2\,\frac{l_m^2}{l_z^2}\right)\epsilon\right] + \mathcal{D}(\mathrm{k}l_m), \tag{14.74}$$

where E_1, E_2, and E_3 are calibration constants. As for Eq. (14.72), the source term is a linear combination of P_s, P_b, and ϵ. In this closure scheme appears a new length scale l_z that needs to be prescribed to force l_m to vanish at solid boundaries. In the $\mathrm{k}-\epsilon$ model, this is achieved "automatically" if the correct boundary conditions are applied (Burchard & Bolding, 2001). Except for this difference, the two formulations are structurally identical because, in the absence of spatial variations, Eqs. (14.72) and (14.74) are equivalent by virtue of Eq. (14.42). The difference lies in the quantity that is transported by the flow: dissipation in the $\mathrm{k}-\epsilon$ model, $\mathrm{k}l_m$ in the Mellor–Yamada model.

In fact, it is possible to establish a generic evolution equation for $\mathrm{k}^a\epsilon^b$ with two parameters a and b ($a=0$, $b=1$ to recover the $\mathrm{k}-\epsilon$ model and $a=5/2$, $b=-1$ to obtain the $\mathrm{k}-\mathrm{k}l_m$ model). Changing the values of a and b changes the nature of the second quantity that is transported by the flow (Umlauf & Burchard, 2003). Whatever combination is chosen, all such models fall under the label of *two-equation models* and, except for the background mixing length l_z, do not need additional prescribed spatial functions.

Leaving aside more complex closure schemes, we end our description of turbulence modeling with the observation that all closure schemes described here are based on local properties, that is, not using distant information to parameterize Reynolds stresses. These models are called *one-point closure* schemes. Schemes that use information from remote locations to infer local turbulence properties are referred to as two-point closure schemes (e.g., Stull, 1993).

We now return to the notation used in the rest of the book by no longer making a distinction between average flow properties and turbulent properties, so that from here on u stands again for the mean velocity.

14.5 MIXED-LAYER MODELING

The turbulence models presented in the previous two sections are applicable to three-dimensional flows in general. In geophysical fluid dynamics, models can

be simplified by exploiting the small aspect ratio of the flows under investigation (e.g., Umlauf & Burchard, 2005). In particular, the strain-rate tensor can be reduced to

$$\mathbf{D}=\frac{1}{2}\begin{pmatrix}\sim 0 & \sim 0 & \frac{\partial u}{\partial z}\\ \sim 0 & \sim 0 & \frac{\partial v}{\partial z}\\ \frac{\partial u}{\partial z} & \frac{\partial v}{\partial z} & \sim 0\end{pmatrix} \tag{14.75}$$

and the shear production to

$$P_s=\nu_{\mathrm{E}}M^2,\quad M^2=\left(\frac{\partial u}{\partial z}\right)^2+\left(\frac{\partial v}{\partial z}\right)^2, \tag{14.76}$$

in which we took the opportunity to define the Prandtl frequency M. Furthermore, turbulent diffusion is chiefly acting in the vertical direction because of the shorter distances and larger gradients in that direction. On the other hand, the study of flows with small aspect ratios inevitably requires that a larger step size be taken in the horizontal and, consequently, that a series of horizontal subgrid scale processes be handled separately. The effects of these are generally modeled by a horizontal diffusion with diffusion coefficient $\mathcal{A}$:

$$\mathcal{D}()=\frac{\partial}{\partial x}\left(\mathcal{A}\frac{\partial}{\partial x}\right)+\frac{\partial}{\partial y}\left(\mathcal{A}\frac{\partial}{\partial y}\right)+\frac{\partial}{\partial z}\left(\nu_{\mathrm{E}}\frac{\partial}{\partial z}\right). \tag{14.77}$$

It should be clear here that ν_{E} is intending to model actual turbulence, whereas $\mathcal{A}$ is an attempt to take into account processes unresolved in the horizontal, at scales longer than l_m but shorter than the horizontal grid step used in the model.

Assuming a Kolmogorov-type turbulent energy cascade in the horizontal, a possible closure is

$$\mathcal{A}\sim(\Delta x)^{4/3}\epsilon_H^{1/3}, \tag{14.78}$$

directly inspired by $\nu_{\mathrm{E}}\sim l_m^{4/3}\epsilon^{1/3}$ [deduced from Eqs. (14.63) and (14.42)]. For this estimation of $\mathcal{A}$, ϵ_H is the energy dissipation of the horizontally unresolved processes. According to Okubo (1971), this dissipation rate is relatively similar from case to case (Fig. 14.10).

Another subgrid scale parameterization of horizontal processes is directly inspired by the Prandtl model (e.g., Smagorinsky, 1963):

$$\mathcal{A}\sim\Delta x\Delta y\left[\left(\frac{\partial u}{\partial x}\right)^2+\left(\frac{\partial v}{\partial y}\right)^2+\frac{1}{2}\left(\frac{\partial u}{\partial y}+\frac{\partial v}{\partial x}\right)^2\right]^{1/2}. \tag{14.79}$$

In this formulation, the mixing length is replaced by the average grid spacing to ensure that all scales below the grid size are effectively treated as unresolved motions. In view of the factors $\Delta x\Delta y$ appearing in the front of Eq. (14.79)

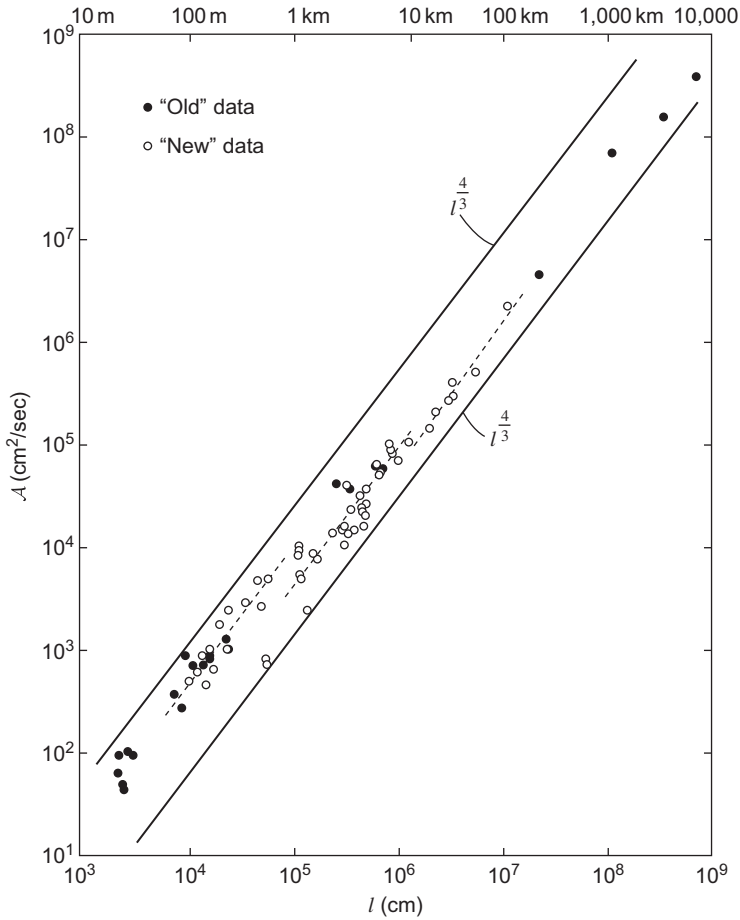

FIGURE 14.10 Horizontal eddy diffusivity as function of cutoff scales in typical geophysical flows (Okubo, 1971).

and the factors Δx^2 and Δy^2 arising in the denominators after the numerical discretization of the horizontal second derivative in the diffusion terms, we can interpret the Smagorinsky formulation as a numerical filter (Section 10.6). This filter acts at the grid resolution with the intensity of the filter cleverly made to depend on the local shear of the flow.

We now leave aside subgrid scale parameterizations because they are less well established than turbulence closure schemes and return to vertical turbulence modeling. In particular, we show that the Prandtl model can be recovered under the assumption of instantaneous and local equilibrium between shear production, buoyancy production, and dissipation (as in stationary and homogeneous turbulence, for example). In this case, the turbulent kinetic energy budget

(14.61) reduces to

$$P_s + P_b = \epsilon. \tag{14.80}$$

For a vertically sheared flow $\langle u \rangle$ in a stratified fluid of stratification frequency N, the equilibrium between production and dissipation yields, using Eqs. (14.63) and (14.42) for a given mixing length l_m,

$$\mathrm{k} = \frac{c_\mu}{\left(c_\mu^0\right)^{3/2}} l_m^2 M^2 (1 - R_f), \tag{14.81}$$

in which the flux Richardson number R_f is defined as

$$R_f = \frac{-P_b}{P_s} = \frac{c'_\mu}{c_\mu} \frac{N^2}{M^2} = \frac{c'_\mu}{c_\mu} Ri. \tag{14.82}$$

The eddy viscosity follows:

$$\nu_\mathrm{E} = \left(\frac{c_\mu}{c_\mu^0} \right)^{3/2} l_m^2 M \sqrt{1 - R_f}. \tag{14.83}$$

We recover the Prandtl closure (14.46) with eddy viscosity now taking into account the stabilizing effect of the stratification via the flux Richardson number. The simplest models are obtained as particular cases of the more complex models.

Further adaptations to mixed-layer flows can be made by introducing so-called *stability functions* into the parameterizations. The derivation of such formulations lies beyond the scope of this chapter, and we only outline here the general approach. The derivation begins with the governing equations for the individual components of the Reynolds stress tensor, obtained by multiplying the governing equations for the velocity fluctuations by other velocity fluctuations and taking their average. Again, higher-order terms demand simplifying hypotheses. Spatial and temporal variations are either neglected under an equilibrium hypothesis similar to Eq. (14.80) or rather heuristically described by an advection-diffusion equation. Depending on the nature of the closure hypotheses made along the way, the end results are so-called *algebraic Reynolds-stress models*. In these models, Reynolds stresses are often appearing in nonlinear algebraic systems that need to be solved to extract the individual stresses. This can be done with some additional approximations, eventually leading to expressions for the Reynolds stresses as functions of mean-flow characteristics. In all cases, formulations of the type (14.73) appear, in which the function c_μ may be quite complicated.

In all algebraic second-order turbulent closure schemes, Reynolds stresses depend on two dimensionless *stability parameters*:

$$\alpha_N = \frac{\mathrm{k}^2}{\epsilon^2} N^2, \quad \alpha_M = \frac{\mathrm{k}^2}{\epsilon^2} M^2. \tag{14.84}$$

Stability functions widely differ based on the various hypotheses used during their derivation (e.g., Canuto et al., 2001; Galperin, Kantha, Mellor & Rosati, 1989; Kantha & Clayson, 1994; Mellor & Yamada, 1982). If $P_s + P_b = \epsilon$ is assumed along the way, so-called *quasi-equilibrium versions* are obtained (Galperin, Kantha, Hassid & Rosati, 1988). These generally exhibit a more robust behavior than other formulations (see Deleersnijder, Hanert, Burchard & Dijkstra, 2008 for a discussion). An example of stability functions are those of Umlauf and Burchard (2005) depicted in Fig. 14.11 and given by

$$\nu_{\mathrm{E}} = c_\mu \frac{\mathrm{k}^2}{\epsilon} \tag{14.85}$$

$$\kappa_{\mathrm{E}} = c'_\mu \frac{\mathrm{k}^2}{\epsilon} \tag{14.86}$$

with the coefficients given by

$$c_\mu = \frac{s_0 + s_1\alpha_N + s_2\alpha_M}{1 + d_1\alpha_N + d_2\alpha_M + d_3\alpha_N\alpha_M + d_4\alpha_N^2 + d_5\alpha_M^2}, \tag{14.87}$$

$$c'_\mu = \frac{s_4 + s_5\alpha_N + s_6\alpha_M}{1 + d_1\alpha_N + d_2\alpha_M + d_3\alpha_N\alpha_M + d_4\alpha_N^2 + d_5\alpha_M^2}. \tag{14.88}$$

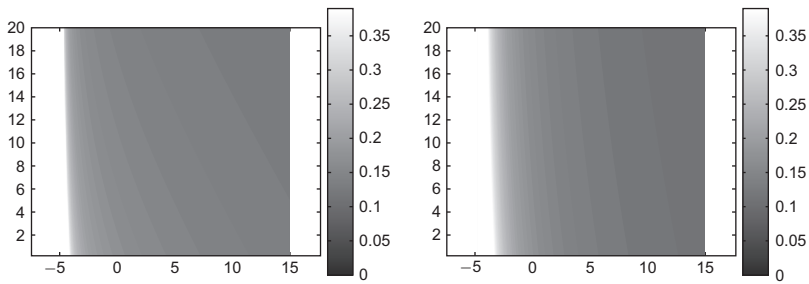

FIGURE 14.11 Stability functions c_μ and c'_μ of Umlauf and Burchard (2005) plotted as functions of α_N and α_M using parameter values given in Table 14.1.

TABLE 14.1 Parameters Used in the Closure Scheme of Canuto et al. (2001)

$s_0 =$	$s_1 =$	$s_2 =$	$s_4 =$	$s_5 =$	$s_6 =$
0.10666	0.01734	−0.00012	0.11204	0.00451	0.00088
$d_1 =$	$d_2 =$	$d_3 =$	$d_4 =$	$d_5 =$	$c_\mu^0 =$
0.2554	0.02871	0.00522	0.00867	−0.00003	0.0768

14.6 PATANKAR-TYPE DISCRETIZATIONS

A turbulent closure scheme does not lend itself to analytical solutions, and numerics are called to the rescue. Before dwelling into numerical discretization, however, it is worth insisting that the equations for turbulent variables are only models obtained after a long series of assumptions. If the derivation is not done with diligence, inconsistencies can arise. Turbulent kinetic energy, for example, must never be negative, but, if the flux Richardson number for some reason begins to exceed one, the equilibrium value of k becomes negative by virtue of Eq. (14.81) and the eddy viscosity Eq. (14.83) ceases to exist. A first constraint on any turbulence closure scheme is therefore that their answers make basic physical sense. For the k model, for example, it should be shown that the solution of Eq. (14.61) is always positive (see Analytical Problem 14.8).

Assuming that the turbulence closure scheme is respecting all physical and mathematical requirements, we should further ensure that subsequent numerical discretization respects these properties (Numerical Exercise 14.2). We may now appreciate why, during the treatment of advection problems (Section 6.4), much discussion was devoted to monotonic behavior. Negative values of a variable that should remain positive can have dramatic effects when nonlinearities are present. The values of the source terms in the equations governing turbulent kinetic energy and dissipation can hint at problems. Occasionally, well-defined mathematical and numerical operations may cause unexpected problems. For example, a quadratic sink for a tracer c with uniform spatial distribution,

$$\frac{\mathrm{d}c}{\mathrm{d}t} = -\mu c^2 \tag{14.89}$$

starting from initial condition c^0 has for solution

$$c(t) = \frac{c^0}{1+\mu t\, c^0}, \tag{14.90}$$

which is well behaved if c^0 is positive but will eventually become unacceptable if c^0 is negative. In the presence of spatial variations, such a problem may be far more difficult to detect but is just as serious.

An implicit treatment of the nonlinear source or sink term would enhance numerical stability and therefore reduce over- or undershooting tendencies (e.g., avoid unphysical negative values), but the numerical cost is the need to invert or solve a nonlinear algebraic equation at each time step. This is tantamount to finding the zeros of a function and can be done with standard iterative methods, Picard, Regula Falsi, Newton–Raphson methods, for example (see Dahlquist & Björck, 1974; Stoer & Bulirsh, 2002). But since the procedure needs to be repeated at each grid point and at each time step, the approach can become quite burdensome. Also problems of robustness in finding roots are not uncommon in view of the large number of times the procedure needs to be repeated. There

is always a risk of no convergence or of convergence toward an unphysical solution.

Patankar (1980) introduced a method that renders the discretization of a nonlinear source term somehow implicit without actually needing to solve a nonlinear algebraic equation. To present his idea, we start from the spatially discretized version of the governing equation for the vector state $\mathbf{x}$ (i.e., the vector consisting of the variables of the model):

$$\frac{\partial \mathbf{x}}{\partial t} = \mathbf{M}(\mathbf{x}) \tag{14.91}$$

where the right-hand side gathers all discretized spatial operators. Such a system can be discretized in time by one of the many methods already presented. The algorithm to update the numerical state variable $\mathbf{x}$ is then of the type

$$\mathbf{A}\mathbf{x}^{n+1} = \mathbf{B}\mathbf{x}^{n} + \mathbf{f}, \tag{14.92}$$

where $\mathbf{A}$ and $\mathbf{B}$ result from the chosen discretization and $\mathbf{f}$ may contain forcing terms, sources, sinks, and boundary conditions. If we now add a decay term to the governing equation

$$\frac{\partial \mathbf{x}}{\partial t} = \mathbf{M}(\mathbf{x}) - \mathbf{K}\mathbf{x} \tag{14.93}$$

with the matrix $\mathbf{K} = \mathrm{diag}(K_i)$ being a diagonal matrix with various decay rates K_i, one for each component of the state vector, an explicit discretization of the decay term then leads to the modified algorithm

$$\mathbf{A}\mathbf{x}^{n+1} = (\mathbf{B} - \mathbf{C})\,\mathbf{x}^{n} + \mathbf{f}, \tag{14.94}$$

in which $\mathbf{C} = \mathrm{diag}(K_i\,\Delta t)$ is, too, a diagonal matrix. Alternatively, an implicit treatment of the decay term would lead to

$$(\mathbf{A} + \mathbf{C})\mathbf{x}^{n+1} = \mathbf{B}\mathbf{x}^{n} + \mathbf{f}. \tag{14.95}$$

The only modification in the calculations is to invert $\mathbf{A} - \mathbf{C}$ instead of $\mathbf{A}$, which does not add much burden since only the diagonal is changed.

Patankar's simple yet powerful trick is to take a nonlinear sink written in a pseudo-linear fashion $-K(c)\,c$. As long as $K(c)$ remains bounded (and positive) for all c, we can always express any sink term in this way simply by defining K accordingly. The discretization then uses at each grid point

$$-K(\tilde{c}_i^{n})\tilde{c}_i^{n+1}, \tag{14.96}$$

which is a consistent discretization. To calculate $\tilde{c}^{n+1}$, all that is required is to modify the system similarly to Eq. (14.95) by adding a term $K_i(\tilde{c}_i^{n})\Delta t$ on the diagonal of $\mathbf{A}$.

The method is simple, but how does this trick help maintain positive values? The explicit discretization applied to a positive value $\tilde{c}^n$ does not ensure positiveness for arbitrary time steps because

$$\tilde{c}^{n+1} = \tilde{c}^n - K(\tilde{c}^n)\Delta t \tilde{c}^n = \left[1 - K(\tilde{c}^n)\Delta t\right]\tilde{c}^n$$

is negative whenever $K(\tilde{c}^n)\Delta t > 1$. In contrast, the Patankar trick replaces the explicit calculation by

$$\tilde{c}^{n+1} = \frac{\tilde{c}^n}{1 + K(\tilde{c}^n)\Delta t},$$

which remains positive at all times. The only requirement for the method to work is that $K(c)$ be bounded for $c \to 0$. Otherwise, upon approaching zero, overflows in the numerical code will occur.

But why not just enforce $K(\tilde{c}^n)\Delta t \leq 1$ by choosing a sufficiently short time step? In so-called *stiff problems*, K varies widely, and the time step being constrained by the largest value of K may have to be excessively short. Unless adaptive time-stepping is used to keep the instances of short time steps to a minimum, it is almost impossible to ensure a sufficiently small time step that keeps $\tilde{c}$ positive at all times without using excessively small time steps during most of the calculations. In coupled nonlinear equations, the stiffness is often difficult to gage, and ecosystem models among others are prone to nonpositive behavior whenever an explicit discretization is used. This is very frustrating because such a problem tends to occur only occasionally. The benefit of the Patankar method is to avoid the time-step penalty in the presence of quickly damped processes.

We now generalize the Patankar method slightly to take into account that sinks decrease values but sources increase them. For a single equation with a source (production term $P \geq 0$) and a sink (destruction term $-K(c)\ c \leq 0$) such that

$$\frac{\mathrm{d}c}{\mathrm{d}t} = P(c) - K(c)\ c, \tag{14.97}$$

a discretization *à la* Patankar would read

$$\tilde{c}^{n+1} = \tilde{c}^n + \Delta t \left\{ \frac{P^n}{\tilde{c}^n} \left[\alpha \tilde{c}^{n+1} + (1-\alpha)\tilde{c}^n\right] - K(\tilde{c}^n)\left[\beta \tilde{c}^{n+1} + (1-\beta)\tilde{c}^n\right] \right\} \tag{14.98}$$

where α and β are implicitness factors. This equation can directly be solved for $\tilde{c}^{n+1}$.

In some problems, the solution of Eq. (14.97) tends toward an equilibrium solution c^*, such that $P(c^*) = K(c^*)\ c^*$, without oscillating around this equilibrium. It is relatively easy to show that this is the case if

$$P(c) \lessgtr K(c)c \quad \text{for} \quad c \gtrless c^*. \tag{14.99}$$

It is then possible to show (Numerical Exercise 14.8) that a numerical solution that keeps concentration values positive and converges toward the equilibrium value c^* without oscillation is guaranteed as long as

$$\frac{1}{\Delta t} \geq \frac{P - Kc}{c^* - c} + \frac{\alpha P - \beta K c}{c}. \tag{14.100}$$

To obtain the least restrictive time step, the best choice is $\alpha = 0$, $\beta = 1$. For example with $P = c^r$ and $K = c^r$, the equilibrium is $c^* = 1$ for any value $r > 0$. If $\alpha = 0$ and $\beta = 1$, the Patankar scheme yields steady convergence toward this value for arbitrary large time steps.

The present example is not an academic one because the perceptive reader may have realized that $r = 1/2$ corresponds to the typical source/sink term in a turbulence closure scheme with fixed mixing length (Section 14.3). The case $r = 1$ arises with the logistic equation encountered in the modeling of biological processes.

The method outlined here has been adapted to a set of coupled equations, ensuring conservation between components and higher-order convergence than the Euler scheme shown here (Burchard, Deleersnijder & Meister, 2003, 2005). Such an approach is of special interest in ecosystem models that include transport.

14.7 WIND MIXING AND PENETRATIVE CONVECTION

Like mixing, turbulence in stratified fluids requires work against buoyancy forces, and stratification thus acts as a moderator of turbulence. This situation can be expressed quantitatively by applying to turbulence some of the concepts derived earlier, particularly the notion of mixing depth, as expressed by Eq. (14.6),

$$\Delta H = \frac{\rho_0 (U_1 - U_2)^2}{2g(\rho_2 - \rho_1)}. \tag{14.101}$$

An important measure of turbulence is the *friction velocity* u_*, a measure of the turbulent velocity fluctuations.[9] Thus, locally horizontal velocities are expected to differ by values on the order of u_*, and the numerator of Eq. (14.101) could be replaced by the dimensionally equivalent expression $\rho_0 u_*^2$. Likewise, the difference $(\rho_2 - \rho_1)$ can be interpreted as a local turbulent density fluctuation and the product $u_*(\rho_2 - \rho_1)$ as a measure of the vertical density flux $\overline{w'\rho'}$ (where primes denote turbulent fluctuation and an overbar indicates some average). The introduction of those quantities transforms Eq. (14.101) into a turbulent

[9]The attribute *friction* reflects the historical heritage of turbulent boundary-layer theory and does not imply that friction is of great importance here.

analogue:

$$L = \frac{\rho_0 u_*^3}{\mathcal{K} g \overline{w'\rho'}}. \tag{14.102}$$

This length scale represents the depth of fluid to which stratification confines eddies of strength u_*. It is called the *Monin–Obukhov length* in honor of the two Soviet oceanographers who, in 1954, first pointed to the importance of this scale in the study of stratified turbulence. In the denominator, the factor $\mathcal{K}$ is the von Kármán constant ($\mathcal{K} = 0.41$), which is traditionally introduced to facilitate mathematical development in boundary-layer applications and which was first encountered in Section 8.1.1.

If density variations are entirely due to temperature stratification, then the flux $\overline{w'\rho'}$ is equal to $-\alpha\rho_0\overline{w'T'}$, where α is the coefficient of thermal expansion and T' is the temperature fluctuation. Because this is often the case, the Monin–Obukhov length is customarily defined as

$$L = \frac{u_*^3}{-\mathcal{K}\alpha g\, \overline{w'T'}}. \tag{14.103}$$

14.7.1 Wind Mixing

As an application, consider the development of a turbulent mixed layer in the upper ocean under the action of a wind stress (Fig. 14.12). Let us assume that, initially, the ocean stratification is characterized by a uniform stratification frequency N, so that the density increases linearly with depth according to

$$\rho = -\frac{\rho_0 N^2}{g} z, \tag{14.104}$$

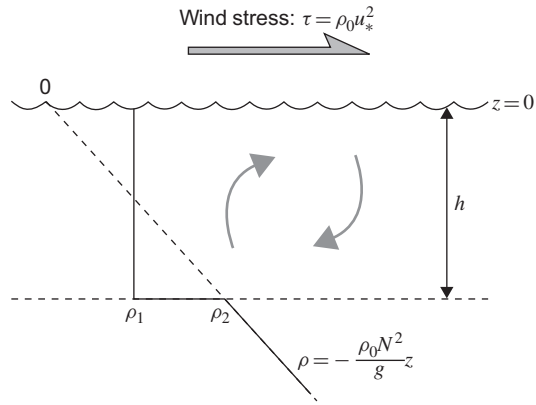

FIGURE 14.12 Development of a mixed layer in the ocean under the action of a wind stress.

where z is the vertical coordinate measured negatively downward ($z=0$ is the surface) and ρ is the density departure from the reference density ρ_0, the initial surface density. After sometime t, this stratification has been partially eroded, and a mixed layer of depth h has developed (Fig. 14.12). In this layer, the density has been homogenized and, in the absence of surface heating, evaporation, and precipitation, has become the average density that initially existed over that depth:

$$\rho_1 = \frac{\rho_0 N^2 h}{2g}.$$

Below the mixed layer, density is still unchanged, $\rho_2 = \rho(z=-h) = \rho_0 N^2 h/g$, and there exists a density jump

$$\Delta\rho = \rho_2 - \rho_1 = \frac{\rho_0 N^2 h}{2g}. \tag{14.105}$$

Mixing has caused upwelling of denser waters and downwelling of lighter waters, thus raising the level of potential energy. The energy gain by time t is

$$\begin{aligned} PE &= \int_{-h}^{0} \rho_1 g z \, \mathrm{d}z - \int_{-h}^{0} \rho g z \mathrm{d}z \\ &= \frac{1}{12} \rho_0 N^2 h^3. \end{aligned} \tag{14.106}$$

Therefore, potential energy increases at the rate

$$\frac{\mathrm{d}PE}{\mathrm{d}t} = \frac{1}{4} \rho_0 N^2 h^2 \frac{\mathrm{d}h}{\mathrm{d}t}. \tag{14.107}$$

The supply of energy is provided by the surface wind. If the wind stress is τ, the turbulent friction velocity u_* is given by Eq. (8.1) (see also Kundu, 1990, Section 12.11):

$$\tau = \rho_0 \, u_*^2, \tag{14.108}$$

and the rate of work performed by τ on fluid particles with typical velocities u_* is proportional to τu_* or $\rho_0 u_*^3$. Introducing a coefficient of proportionality m to account for the exact rate of work minus the portion diverted to kinetic-energy production (which eventually dissipates), we state: $\mathrm{d}PE/\mathrm{d}t = m\rho_0 u_*^3$, or by virtue of Eq. (14.107),

$$N^2 h^2 \frac{\mathrm{d}h}{\mathrm{d}t} = 4 m u_*^3. \tag{14.109}$$

Observations and laboratory experiments suggest $m = 1.25$. This last equation can be readily integrated to obtain the instantaneous mixed-layer depth:

$$h = \left(\frac{12 m u_*^3}{N^2} t \right)^{1/3}. \tag{14.110}$$

Of some interest here is the evaluation of the Monin–Obukhov length. As the layer erodes the underlying stratification at the rate $\mathrm{d}h/\mathrm{d}t$, turbulence must overcome the density jump $\Delta\rho$, causing a density flux at the base of the mixed layer of magnitude

$$\begin{aligned} \overline{w'\rho'} &= \frac{\mathrm{d}h}{\mathrm{d}t} \Delta\rho \\ &= \frac{2 m \rho_0 u_*^3}{g h}, \end{aligned} \tag{14.111}$$

by virtue of Eqs. (14.105) and (14.109). Based on this local flux value, the Monin–Obukhov length (14.102) is found to be

$$L = \frac{1}{2m\mathcal{K}} h. \tag{14.112}$$

With the numerical values $\mathcal{K} = 0.40$ and $m = 1.25$, L is exactly h. The exact identity between L and h is fortuitous (especially since $\mathcal{K}$ is closer to 0.41 than 0.40), but it remains that the depth of the turbulent mixed layer is on the order of the Monin–Obukhov length, thus imparting a direct physical meaning to the latter.

The preceding considerations illustrate but one aspect of the development of a mixed layer in the upper ocean. Much work has been done on this problem, and the reader desiring additional information is referred to the book edited by Kraus (1977) for a review and to the article by Pollard, Rhines and Thompson (1973) for a particularly clear discussion of Coriolis effects and of the relevance of the Richardson number. See also Section 8.7.

Considerations of mechanically induced mixing in the lower atmosphere and above the ocean floor can be found, respectively, in Sorbjan (1989, Section 4.4.1) and in Weatherly and Martin (1978). A review of laboratory experiments and associated theories is provided by Fernando (1991).

14.7.2 Penetrative Convection

Convection is defined as the process by which vertical motions modify the heat distribution in the system. In the example at the end of the previous subsection, the stirring of the upper ocean layer is caused by the mechanical action of the wind stress, and convection is said to be forced. Natural, or free, convection arises when the only source of energy is of thermal origin, such as an imposed temperature difference or an imposed heat flux, and the motions associated with

the convective process derive their energy from the work generated by buoyancy forces as warm fluid rises and cold fluid sinks.

A common occurrence of natural convection in geophysical fluids is the development of an unstable atmospheric boundary layer (Sorbjan, 1989). During daytime, the solar radiation traverses the atmosphere and reaches the earth (ground or sea), where it is absorbed. The earth reemits this radiation in the infrared range, thus effectively heating the atmosphere from below. As a result, the lowest level of the atmosphere is usually an unstable, convective region, called the *atmospheric boundary layer*. The existence of this layer is very beneficial to humans because of the ventilation it causes. When the atmosphere is stably stratified down to the ground, a situation called *inversion*, the air is still and uncomfortable; moreover, if there is a source of pollution, this pollution stagnates and can become harmful. Such is the situation in Los Angeles (USA) when smog occurs (Stern, Boubel, Turner & Fox, 1984).

The intensity of stirring motions in natural convection depends, obviously, on the strength of the thermal forcing, as well as on the resistance of the fluid to move (viscosity) and to conduct heat (conductivity). A traditional example is convection in a fluid layer of height h confined between two horizontal rigid plates and heated from below. The forcing is the temperature difference ΔT between the two plates, the lower one being the hotter of the two. At low temperature differences, the viscosity ν and heat diffusivity κ_T of the fluid prevent convective motions, the fluid remains at rest, and the heat is carried solely by molecular diffusion (conduction). As the temperature difference is increased, everything else remaining is unchanged, the hot fluid at the bottom will eventually float upward, and the cold fluid will sink from above.

If viscosity is the limiting factor, the amplitude of the convective velocities, w_*, can be estimated from a balance between the upward buoyancy force $-g\rho'/\rho_0 \sim \alpha g \Delta T$ (where α is the coefficient of thermal expansion) and the retarding frictional force $\nu \partial^2 w/\partial z^2 \sim \nu w_*/h^2$, yielding:

$$w_* \sim \frac{\alpha g \Delta T h^2}{\nu}. \tag{14.113}$$

Comparing the convective heat flux $\overline{w'T'} \sim w_* \Delta T \sim \alpha g \Delta T^2 h^2/\nu$ to the conductive flux $\kappa_T \partial T/\partial z \sim \kappa_T \Delta T/h$, we form the ratio

$$Ra = \frac{\alpha g \Delta T^2 h^2/\nu}{\kappa_T \Delta T/h} = \frac{\alpha g \Delta T h^3}{\nu \kappa_T}, \tag{14.114}$$

which is known as the *Rayleigh number*, in honor of British scientist Lord Rayleigh,[10] who first studied this problem quantitatively (1916).

[10] Rayleigh was a contemporary of Kelvin. See the joint photograph at end of Chapter 9.

Convection occurs, theories show (Chandrasekhar, 1961), when this number exceeds a critical value, which depends on the nature of the boundary conditions. For a fluid confined between two rigid plates, the critical Rayleigh number is $Ra = 1708$. At values slightly above the threshold, convection organizes itself in parallel two-dimensional rolls or in packed hexagonal cells. At higher values of the Rayleigh number, erratic time-dependent motions develop, and convection appears much less organized.

Geophysical fluids almost always fall in this last category because of the large heights involved and the small values of molecular viscosity and conductivity of air and water. In the atmospheric boundary layer, where the Rayleigh number typically exceeds 10^{15}, convection is manifested by the intermittent formation near the ground of warm pockets of air, called *thermals*, which then rise through the convective layer; the circuit is completed by a weak subsidence of colder air between the rising thermals. In such a situation, viscosity and heat diffusivity play secondary roles, and the main characteristics of the flow do not depend on them.

As an application, consider the development of an atmospheric boundary layer from an initial, stable stratification under the action of a constant heat flux supplied by the ground (Fig. 14.13). At time $t = 0$, the air is assumed linearly stratified with potential-temperature profile given by

$$\bar{T}(z) = T_0 + \Gamma z, \tag{14.115}$$

where T_0 is the initial potential temperature at the ground and Γ is the vertical potential-temperature gradient, corresponding to a stratification frequency $N = (\alpha g \Gamma)^{1/2}$. The upward heat flux at the ground, denoted by $\rho_0 C_p Q$, is assumed constant. After some time t, convection has eroded the stratification up to a height $h(t)$. The temperature $T(t)$ in the convective layer varies according

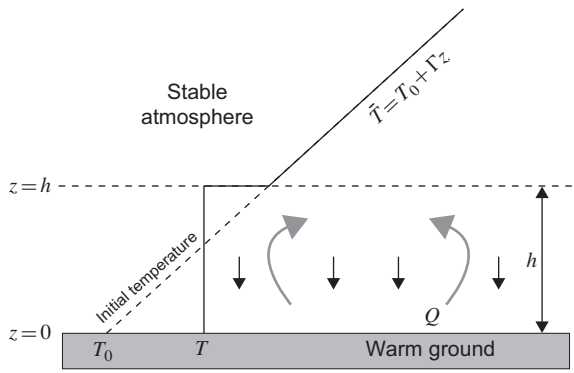

FIGURE 14.13 An unstable atmospheric boundary layer. The heat supplied at the ground surface generates convection, which progressively erodes the stratification above.

to the instantaneous distribution of thermals but, on the average, appears to be nearly constant with height. The heat budget for the intervening time requires that the change in heat content of the affected fluid be equal to the accumulated heat received from the ground,

$$\rho_0 C_p \int_0^h (T-\bar{T})\,\mathrm{d}z = \int_0^t \rho_0 C_p Q\,\mathrm{d}t, \tag{14.116}$$

and provides a first relation between the height of the convective layer and its temperature:

$$h(T-T_0) - \frac{1}{2}\,\Gamma h^2 = Q\,t. \tag{14.117}$$

Another relation between these two variables arises from the mechanical-energy budget. Because there is no source of mechanical energy, the sum of the kinetic and potential energies of the system decays with time under the action of frictional forces. In first approximation, to be verified a posteriori, the amount of kinetic energy and energy loss to friction are insignificant contributions compared with the potential-energy changes undergone by the system. So, it suffices to state in first approximation that potential energy, per unit area, at time t is equal to that at the initial time:

$$\int_0^{h(t)} \rho_0 \alpha T g z\,\mathrm{d}z = \int_0^{h(t)} \rho_0 \alpha \bar{T} g z\,\mathrm{d}z, \tag{14.118}$$

which yields

$$T - T_0 = \frac{2}{3}\Gamma h. \tag{14.119}$$

Physically, this implies that the temperature rise at the ground is two-thirds of the temperature change over the height h according to the initial temperature gradient (Fig. 14.13). Oddly enough, the temperature in the upper third of the convective layer has decreased, whereas the fluid undergoes an overall heating. This is explained by the upward motion of colder air from below.

Together, Eqs. (14.117) and (14.119) provide the temporal evolution of the thickness and potential temperature of the atmospheric boundary layer:

$$h = \sqrt{\frac{6Qt}{\Gamma}} \tag{14.120}$$

$$T = T_0 + \sqrt{\frac{8\Gamma Q t}{3}}. \tag{14.121}$$

The atmospheric boundary layer thus grows according to the square root of time. This progressive erosion of the ambient stratification by convective motions is termed *penetrative convection*.

We are now in a position to estimate the contribution of kinetic energy. Because convection is accomplished by thermals that rise over the entire extent of the layer, the convective overturns are as deep as the layer itself, and the Monin–Obukhov length must be comparable to the layer thickness. Equating these two quantities, we write

$$\frac{w_*^3}{\mathcal{K}\alpha g Q} = h, \tag{14.122}$$

where the symbol w_* replaces u_* to indicate that the turbulent motions are not mechanically induced (such as by a shear stress) but are of thermal origin. This equality yields a measure of the turbulent velocity w_*:

$$w_* = (\mathcal{K}\alpha g h Q)^{1/3}, \tag{14.123}$$

which supersedes Eq. (14.113) when the Rayleigh number is so high that viscosity is no longer the dominant parameter. The kinetic energy is then estimated to be $\rho_0 w_*^2 h/2$, and its ratio to the instantaneous potential energy $\rho_0 \alpha g (T - T_0) h^2/2$ is

$$\frac{KE}{PE} \sim (Nt)^{-2/3}, \tag{14.124}$$

with the numerical coefficients discarded. In this last expression, $N = (\alpha g \Gamma)^{1/2}$ is the frequency of the undisturbed stratification. Because $1/N$ is typically on the order of a few minutes while the atmospheric boundary layer develops over hours, the product Nt is large, and we can justify the earlier neglect of the kinetic-energy contribution to the overall energy budget. A fortiori, the decay rate of kinetic energy by frictional forces is also unimportant in the overall energy budget. Finally, it is worth noting that if w_* is the velocity scale of the rising thermals, the heat flux $Q = \overline{w'T'}$ is carried by those thermals with their temperature differing from that of the descending fluid approximately by $T_* = Q/w_*$.

The preceding application is but a simple example of convection in the atmosphere. Generally, convective motions in the atmospheric boundary layer are affected by numerous factors, including winds, which they in turn affect. A sizable body of knowledge has been accumulated on the physics of the atmospheric boundary layer, and the interested reader is referred to Sorbjan (1989) or to Garratt (1992).

In numerical models, convection may or may not be resolved depending on its length scale compared with the size of the system. When convection occurs

at scales too small to be resolved, numerical convective adjustment is used (see Section 11.4).

ANALYTICAL PROBLEMS

14.1. A stratified shear flow consists of two layers of depth H_1 and H_2 with respective densities and velocities ρ_1, U_1 and ρ_2, U_2 (left panel of Fig. 14.1). If the lower layer is three times as thick as the upper layer and the lower layer is stagnant, what is the minimum value of the upper layer velocity for which there is sufficient available kinetic energy for complete mixing (right panel of Fig. 14.1)?

14.2. In the ocean, a warm current ($T = 18°C$) flows with a velocity of 10 cm/s above a stagnant colder layer ($T = 10°C$). Both layers have identical salinities, and the thermal-expansion coefficient is taken as $2.54 \times 10^{-4}\ K^{-1}$. What is the wavelength of the longest unstable wave?

14.3. Formulate the Richardson number for a stratified shear flow with uniform stratification frequency N and linear velocity profile, varying from zero at the bottom to U at a height H. Then, relate the Richardson number to the Froude number and show that instabilities can occur only if the Froude number exceeds the value 2.

14.4. In an oceanic region far away from coasts and strong currents, the upper water column is stably stratified with $N = 0.015\ s^{-1}$. A storm passes by and during 10 hours exerts an average stress of $0.2\ N/m^2$. What is the depth of the mixed layer by the end of the storm? (For seawater, take $\rho_0 = 1028\ kg/m^3$.)

14.5. An air mass blows over a cold ocean at a speed of 10 m/s and develops a stable potential-temperature gradient of 8°C per kilometer in the vertical. It then encounters a warm continent and is heated from below at the rate of $200\ W/m^2$. Assuming that the air mass maintains its speed, what is the height of the convective layer 60 km inshore? What is then a typical vertical velocity of convection? (Take $\rho_0 = 1.20\ kg/m^3$, $\alpha = 3.5 \times 10^{-3}\ K^{-1}$, and $C_p = 1005\ J\ kg^{-1}\ K^{-1}$.)

14.6. For the growing atmospheric boundary layer, show that thermals rise faster than the layer grows ($w_* > dh/dt$) and that thermals have a temperature contrast less than the temperature jump at the top of the layer [$T_* < (T - T_0)/2$].

14.7. Why should eddy viscosity be considered positive? What happens to the energy budget if $\nu_E \leq 0$?

14.8. Consider the following governing equation for the turbulent kinetic energy k:

$$\frac{\partial \mathsf{k}}{\partial t} = \nu_{\mathrm{E}} M^2 - \kappa_{\mathrm{E}} N^2 - \epsilon$$

with Eqs. (14.63), (14.64), and (14.42) for fixed M^2, N^2, l_m and $c_\mu / c'_\mu = 0.7$. Show that the solution is always nonnegative as long as the initial value of k is nonnegative.

NUMERICAL EXERCISES

14.1. Assuming the turbulent kinetic energy budget is dominated by local production and dissipation, how would you define a staggered grid for a one-dimensional model of a water column?

14.2. Implement a numerical method that keeps the turbulent kinetic energy k positive for decaying turbulence in a homogeneous k–ϵ model.

14.3. Show that for turbulence in statistical equilibrium, stability functions depend only on the Richardson number.

14.4. Revisit the estimate of the computing power needed to simulate geophysical fluid dynamics down to the dissipation range, with microscale in mind and for a typical value of $\epsilon = 10^{-3}$ W/kg.

14.5. What to you think that the requirement should be on the vertical grid spacing Δz compared with l_m?

14.6. Implement a 1D model including a k–ϵ closure scheme. If help is needed, look at `kepsmodel.m`, but do not cheat.

14.7. Use the program developed in Numerical Exercise 14.6 or `kepsmodel.m` to simulate the case of wind-induced mixing of Analytical Problem 14.4. In particular, consider the temporal evolution of the surface velocity in hodograph form (u, v axes), with or without Coriolis force. Then repeat the exercise but do not allow the wind to stop. Again, compare the situations with or without Coriolis force. To do so, trace in both cases, the mixed-layer depth evolution as shown in Fig. 14.14.

14.8. Prove that Eq. (14.100) is the sufficient condition to ensure that the numerical solution obtained with Eq. (14.98) converges toward the equilibrium value c^*, remains positive, and never crosses the value $c = c^*$.

14.9. Simulate a convection case in the ocean with a uniform initial stratification of $N = 0.015\,\mathrm{s}^{-1}$. Then apply a destabilizing heat loss of 200 W/m^2

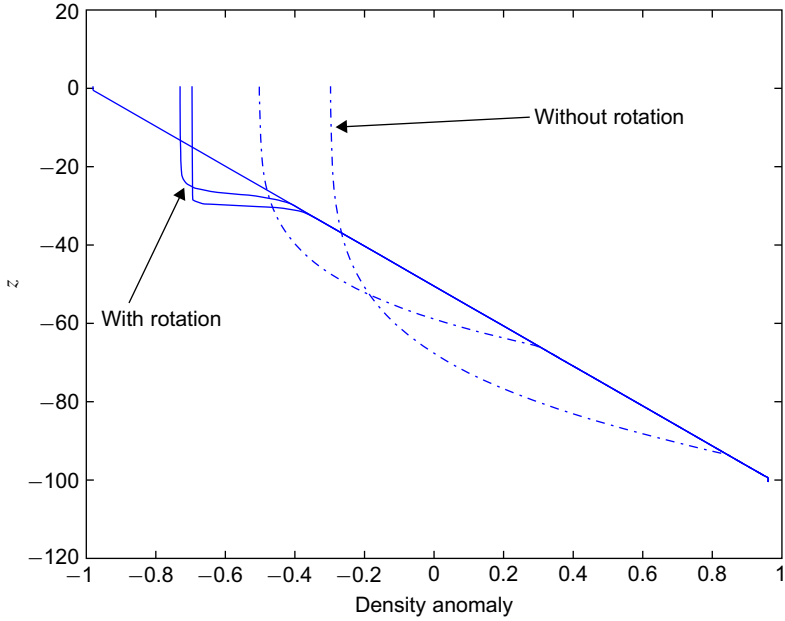

FIGURE 14.14 A uniform stratification being erased by a constant surface wind. In the absence of rotation, the mixed layer deepens (two profiles are shown in dashed lines). With rotation, the mixed layer stabilizes (two profiles in solid lines), and the pycnocline is sharper. See Numerical Exercise 14.7.

at the surface. Translate the heat flux into density anomaly flux and use the 1D model without rotation. Start from rest. Implement a method to detect the mixed-layer depth and trace its evolution over time. Do the same for the wind-mixing case of Numerical Exercise 14.7. Compare with the theoretical results of Section 14.7.

Lewis Fry Richardson
1881–1953

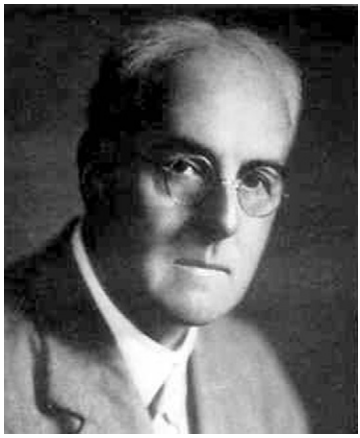

Unlike many scientists of his generation and the next, Lewis Fry Richardson did not become interested in meteorology because of a war. On the contrary, he left his secure appointment at the Meteorological Office in England during World War I to serve in a French ambulance convoy and tend the wounded. After the war, he returned to the Meteorological Office (see historical note at the end of Chapter 1), only to leave it again when it was transferred to the Air Ministry, deeply convinced that "science ought to be subordinate to morals."

Richardson's scientific contributions can be broadly classified in three categories: finite-difference solutions of differential equations, meteorology, and mathematical modeling of nations at war and in peace. The marriage of his first two interests led him to conceive of numerical weather forecasting well before computers were available for the task (see Section 1.9). His formulation of the dimensionless ratio that now bears his name is found in a series of landmark publications during 1919–1920 on atmospheric turbulence and diffusion. His mathematical theories of war and peace were developed in search of rational means by which nations could remain in peace.

According to his contemporaries, Richardson was a clear thinker and lecturer, with no enthusiasm for administrative work and a preference for solitude. He confessed to being "a bad listener because I am distracted by thoughts." (*Photo by Bassano and Vandyk, London*)

George Lincoln Mellor
1929–

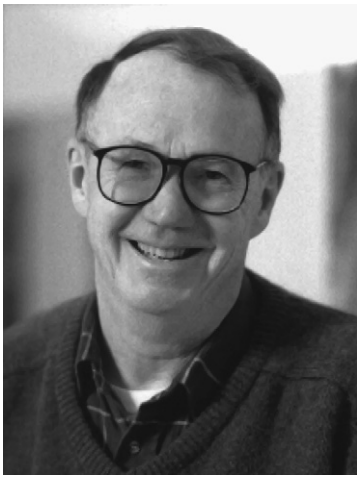

George Mellor's career has been devoted to fluid turbulence in its many forms. His early interest in aerodynamics of jet engines and turbulent boundary layers soon yielded to a stronger interest in the turbulence of stratified geophysical flows. In the mid 1970s, he developed with Tetsuji Yamada a closure scheme to model turbulence in stratified flows, which is being used worldwide in atmospheric and oceanographic applications. Their joint 1982 publication in *Reviews of Geophysics and Space Physics* is one of the most widely cited papers in its field.

Mellor is also known as the architect of the so-called *Princeton Ocean Model*, nicknamed POM, which is used the world over to simulate ocean dynamics, particularly in coastal regions and wherever turbulent mixing is significant. He is the author of the textbook "Introduction to Physical Oceanography" (American Institute of Physics, 1996). (*Photo courtesy of Princeton University*)